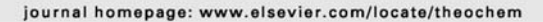


Contents lists available at ScienceDirect

Journal of Molecular Structure: THEOCHEM





A performance study of density functional theory with empirical dispersion corrections and spin-component scaled second-order Møller-Plesset perturbation theory on adsorbate-zeolite interactions

Pornthip Tongying, Yuthana Tantirungrotechai*

National Center of Nanotechnology (NANOTEC), National Science and Technology Development Agency, Pathumthani 12120, Thailand

ARTICLE INFO

Article history:
Received 14 September 2009
Received in revised form 13 December 2009
Accepted 11 January 2010
Available online 18 January 2010

Keywords: Zeolite Density functional theory Dispersion correction Double-hybrid density functional Spin-component scaled MP2

ABSTRACT

Density functional theory models, PBE, BLYP, B3LYP, B2PLYP and mPW2PLYP, with empirical dispersion corrections and the spin-component scaled second-order Møller—Plesset perturbation theory, SCS-MP2, were tested against the benchmarking adsorbate—zeolite models of Zhao and Truhlar. The van der Waals dispersion correction improves the binding energy significantly for all considered exchange—correlation functionals. The adsorption energies from the density functional theory with double perturbation correction with dispersion term, B2PLYP-D and mPW2PLYP-D, match the CCSD(T) results extrapolated to the complete-basis set even better. The mean unsigned errors of counterpoise-corrected binding energy of B2PLYP-D and mPW2PLYP-D methods are only 0.17 and 0.08 kcal/mol, respectively. The double-hybrid density functional with dispersion corrections should be used for high accuracy zeolite computation. Alternatively, the counterpoise-uncorrected SCS-MP2 calculation can be used to estimate the binding energy due to some cancellation of errors. Finally, an importance of the speed-up algorithms such as RI-MP2, RIJCOSX and RI-JR of the methods considered in this work was demonstrated by using 3T and 16T zeolite cluster models.

1. Introduction

Several new exchange-correlation functionals appear in the literature every now and then. A good example is the recent development towards developing the meta-GGA functional which performs better than the popular B3LYP functional in all aspects. Truhlar and coworkers have developed families of excellent exchange-correlation functionals for such general purpose [1]. A notable example is the family of MO6 functionals [2,3]. Alternatively, a pragmatic view on improving the DFT performance also exists in literatures. A notable example is the empirical modification to the density functional theory by Grimme [4,5].

By adopting the idea of the Hartree-Fock dispersion correction

By adopting the idea of the Hartree-Fock dispersion correction model by Ahlrichs et al. [6], Grimme proposed the addition of damped, atom-pairwise R^{-6} term to the energy expression to recover the long-range dispersion behavior

$$E_{\text{DFT-D}} = E_{\text{KS-DFT}} + E_{\text{disp}} = E_{\text{KS-DFT}} - s_6 \sum_{i=1}^{N_{\text{eff}}} \sum_{j=i+1}^{N_{\text{eff}}} \frac{C_6^{ij}}{R_{ij}^{e}} f_{\text{damp}}(R_{ij})$$

0166-1280/\$ - see front matter © 2010 Elsevier B.V. All rights reserved. doi:10.1016/j.theochem.2010.01.020

This is called the density functional theory with van der Waals dispersion correction or DFT-D. The empirical parameters, s_6 and Ce. for the model were fitted for a number of well-known exchange-correlation functionals. This has been proven very successful and received much attention recently [7-10]. To extend this practical view, Grimme also proposed another semiempirical density functional model which incorporates a fragment of non-local correlation by the second-order perturbative correction (PT2) into the energy expression. This model is termed the double-hybrid functional model (DHDF) [11]. The combinations of the PT2 non-local correction and LYP correlation functional with the B88 or mPW exchange functionals result in the B2PLYP and mPW2PLYP models. respectively. Exclusive studies by Grimme and coworkers indicate that the mPW2PLYP model performs slightly better than the B2PLYP model [12,13]. By combining the two original ideas together, Schawbe and Grimme later proposed an addition of van der Waals correction term to DHDF [14]. The B2PLYP-D and mPW2PLYP-D models are by far the best successful models. However, the applications so far are mainly on biological relevant and organic systems [15,16].

In this work we test several empirical density functional models against the adsorbate-zeolite system. We consider the zeolite system due to its wide practical application in petrochemical industry. Svelle et al. employed the PBE and PBE-D with periodic DFT models for the adsorption of methanol and alkenes in H-ZSM-5 zeolite [17]. They observed an increase in binding energy which improves the calculated results when the dispersion correction is included to

Corresponding author.
 E-mail addresses: tongying.p@gmail.com (P. Tongying), yuthana@nanotec.or.th. yt203y@gmail.com (Y. Tantirungrotechai).

the periodic PBE model. Zhao and Truhlar performed a benchmark test on the binding energy of zeolite system [18]. Adopting the 3T H¹ zeolite bare cluster, they assessed the binding energy calculated by well-known functionals and their M06 exchange-correlation functionals and compared them with the result of the CCSD(T) method extrapolated to the basis set limit. The M06 family, notably M06-2X, performs better than the popular B3LYP functional and several other common functionals. By using the same model and high-quality benchmark as Zhao and Truhlar, we can assess the performance of Grimme's empirical density functional models on the adsorbate-zeolite system with the same standard.

We also considered the spin-component scaled MP2 (SCS-MP2) method in this investigation [19,20]. This wavefunction-based method scales the parallel spin and anti-spin second-order perturbation contributions to the electron correlation. Antony and Grimme conducted a SCS-MP2 assessment on non-covalent interaction energies of 165 biological relevant complexes (JSCH 2005 database) [20]. The SCS-MP2 perform statistically well in that system compared with the original MP2 calculation. They observed that the effects of basis-set superposition error and basis set incompleteness almost cancel each other when using the triple-zeta basis set. The use of SCS-MP2 in large systems is also favored not only due to its accuracy but also due to this cancellation of errors. It is therefore interesting to see if that behavior is extendable to the adsorbate-zeolite system which is not included in their test.

2. Methods

The zeolite was modeled as 3T H+ bare cluster (Hz). The adsorbates consist of CH₄, C₂H₄, C₂H₆, C₂H₄ in alkoxide form and H₂O. These molecules expand the range of nonpolar to polar compounds. The original zeolitic structures were reported by Zhao and Truhlar [18]. These were optimized at the MP2/6-311+G(2df,2p) level. The binding energies of all adsorbates were calculated at the PBE, BLYP, B3LYP, B2PLYP and mPW2PLYP with and without the van der Waals dispersion correction, and at the SCS-MP2 levels. The resolution of identity (RI) approximation was applied for the PBE and BLYP functionals. The Ahlrichs' TZVP basis set with a new set of polarization functions (def2-TZVP) was used in the calculations [21,22]. The triple-zeta quality basis set was chosen because the second-order perturbative correction is included in some studied methods. All calculations were performed by using the ORCA version 2.6.35 program [23]. A large grid setting ('Grid6') was used for the DFT calculations to eliminate grid-size errors. The binding energy was defined as the equilibrium binding energy (D_e) . The counterpoise correction (CP) was also applied to the binding energy to remove the basisset superposition error (BSSE). The calculated binding energies were compared with the best estimate binding energies which are the

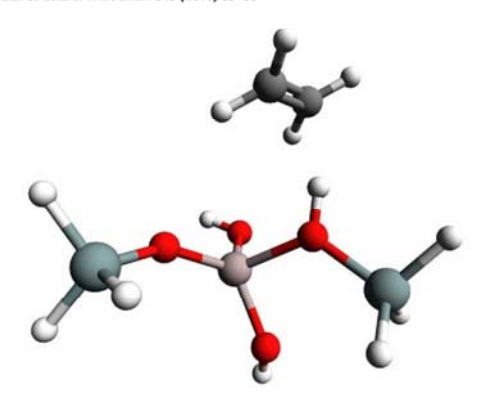


Fig. 1. Adsorbate. . H'3T zeolite complex geometry which adsorbate is π -C₂H₄ in this figure. This figure was generated by using Avogadro (http://avogadro.openmolecules.net).

CCSD(T) extrapolated to the complete basis limit. The mean unsigned errors (MUE) were estimated for all methods.

3. Results and discussion

Fig. 1 displays representative adsorbate...3T H* zeolite model system as suggested by Zhao and Truhlar [18]. Table 1 reports the equilibrium binding energies of the adsorbate-zeolite model systems for considered methods with or without the Boys-Bernadi counterpoise correction. The counterpoise correction is necessary in this case. There are some slight differences in our BLYP, PBE and B3LYP results with those reported by Zhao and Truhlar. These discrepancies are due to different settings of the program including the grid size, the basis set and the resolution-of-identity algorithm (BLYP and PBE).

For saturated hydrocarbons, the PBE, BLYP and B3LYP functionals underestimated the binding energies. For example, the popular B3LYP model underestimates binding energies of CH₄, C₂H₆ and C₂H₄ adsorbates by 2.50, 4.43, 3.71 kcal/mol which is 73%, 98%, 47% of total binding energies. Without the dispersion correction, the PBE functional already performs reasonable in predicting the adsorbate-zeolite binding energy. Its performance is more superior than the BLYP functional given the fact that both are GGA functionals. The BLYP functional even predicts a negative binding energy in C₃H₆. ...Hz system.

Table 1
The binding energy (D_e) and counterpoise-corrected binding energy (D_e -CP) of adsorbate-H*3T zeolite model in kcal/mol. The def2-TZVP basis set was used for all calculations. The best estimate is the CCSD(T) extrapolated to the complete-basis set limit [18].

Method CH_4Hz D_e D_e -CP	lz	C ₂ H ₆ H	z	πC ₂ H ₄ .	.Hz	H ₂ OHz	Z	C ₂ H ₄ alko:	kideHz	Mean er	TOT	
	De	D _e -CP	De	D _e -CP	De	D _e -CP	De	D _e -CP	De	D _e -CP	MUE	MUE-C
Best estimate	3	.45	4	.5	7	.79	14	.97	1	9.51		
RI-PBE	2.41	2.11	2.23	1.75	6.37	5.74	15.50	14.31	19.62	18.27	1.07	1.61
RI-PBE-D	4.79	4.49	6.20	5.72	9.58	8.95	17.91	16.72	24.19	22.83	2.49	1.70
RI-BLYP	0.62	0.32	-0.45	-0.95	3.90	3.23	13.44	12.18	11.68	10.19	4,21	5.05
RI-BLYP-D	4.44	4.13	5.90	5.40	9.04	8.37	17.30	16.04	18.98	17.49	1.30	1.05
B3LYP	1.22	0.95	0.53	0.07	4.67	4.08	13.66	12.63	15.16	13.86	3.00	3.73
B3LYP-D	4.56	4.28	6.08	5.62	9.17	8.57	17.04	16.01	21.55	20.25	1.63	0.90
B2PLYP	2.41	1.75	2.60	1.52	6.49	5.33	14.72	13.05	18.60	15.67	1.08	2.58
B2PLYP-D	4.15	3.50	5.51	4.43	8.84	7.68	16.49	14.82	21,94	19.02	1.34	0.17
mPW2PLYP	3.00	2.38	3.42	2.39	7.20	6.07	15.42	13.78	19.95	17.14	0.60	1.69
mPW2PLYP-D	4.27	3.65	5.54	4.51	8.91	7.78	16.71	15.07	22.38	19.57	1.52	0.08
SCS-MP2	3.20	1.96	4.05	2.11	7.74	5.77	14.32	11.80	19.98	14.81	0.37	2.75

Table 2
Computational times in minute for H₂O...H*3T and H₂O...H*16T zeolite cluster models conducted on a quad core PC machine (Q9450 chip @ 2.66 GHz with 4GB RAM). The 16T-Hz model is a H-Ferrierite cluster model as introduced by Tuma and Sauer [24].

	Average single SCF cycle (min)		MP2 (min)		Total run time (r	min)
	H ₂ O3T-Hz	H ₂ O16T-Hz	H ₂ O3T-Hz	H₂O16T-Hz	H ₂ O3T-Hz	H ₂ O16T-H ₂
SCS-MP2	1	73	37	n.a.	75	n.a.
SCS-MP2 with RI-MP2	1	59	0.2	165	22	1527
B2PLYP	1	54	6	n.a.	24	n.a.
B2PLYP with RI-MP2	1	54	0.3	475	16	1510
B2PLYP with RIJCOSX and RI-MP2	0.3	6	0.3	442	5	561
B3LYP	1	56	-	-	17	1063
B3LYP with RIJCOSX	0.3	6	-	-	4	117
BLYP	0.8	52	-	-	15	996
BLYP with RI-J	0.1	2	-	-	2	34

Upon augmenting the dispersion correction to the original functionals, the binding energies generally increase to be close to the best estimate which is the CCSD(T) binding energy extrapolated to the complete-basis set limit. It is clear that the van der Waals dispersion correction recovers a signification portion of weak interaction energy that is missing in original density functional models and, hence, improves the adsorbate-zeolite binding energy significantly. The dispersion correction seems to overshoot the adsorbate-zeolite binding energy only in the PBE-D functional. Judging from the MUE, the BLYP-D and B3LYP-D models are clearly in favor over the original functionals and should be used in this system to estimate the binding energy. Both models, however, yield similar binding energies. Considering the computational speed-up gained from the RI algorithm, the BLYP-D method might be preferred over B3LYP-D.

The B2PLYP and mPW2PLYP double-hybrid density functionals already performs better than the well-known GGA and hybrid functionals considered in this work. Their counterpoise-uncorrected binding energies matches well with the best estimate. The counterpoise correction, however, reduces their magnitudes. Including the dispersion correction term improves the quality of counterpoise-corrected binding energy significantly. Both counterpoise-corrected B2PLYP-D and mPW2PLYP-D binding energies are in excellent agreement with the best estimate; the average mean unsigned errors of the counterpoise-corrected B2PLYP-D and mPW2PLYP-D binding energies are only 0.17 and 0.08 kcal/mol, respectively. The double-hybrid density functional with dispersion correction can therefore be used as a high quality calculation without resorting to a much more expensive CCSD(T) calculation.

Now we turns to the spin-component scaled MP2 method. This modified MP2 method speeds up the MP2 calculation without compromising its quality. Zhao and Truhlar reported the mean error of MP2 computed with aug-cc-pVDZ, aug-cc-pVTZ and 6-31+C(d,p)basis sets [18]. The SCS-MP2 underestimates the binding energy of saturated hydrocarbon adsorbates but gives a good estimate of π -interaction in ethylene–zeolite system. The counterpoise-corrected SCS-MP2 binding energies are not as accurate as those from double-hybrid density functional models. However, its counterpoise-uncorrected binding energy turns out to be in closer agreement with the best estimate result than the double-hybrid density functional. The SCS-MP2/def2-TZVP method also yields a lower MUE than those from MP2 calculations reported by Zhao and Truhlar [18]. These indicate some cancellation of errors that can be explored in case that one neglects the use of counterpoise correction due to an additional computational cost. This supports what Antony and Grimme observed earlier in biologically relevant systems [20].

For a system of greater size such as isobutene...16T zeolite cluster model that were investigated by Tuma and Sauer [24] and by Zhao and Truhlar [18], its computational cost can be prohibitively expensive, particularly for any methods involving the MP2 calculation. Zhao and Truhlar reported the benchmark data of four forms of isobutene interacting with 16T-Hz cluster model

taken from H-Ferrierite zeolite. The authors found that their set of Minnesota density functionals, M05-2X, M06-2X, M06-L and M06, generally performs better than the MP2/TZVP(P) method. Notable result can also be achieved from the M06-L local functional extrapolated to the complete-basis set. The M06-L functional is an attractive choice since it can be speed up by using the resolution-of-identity algorithm.

Treating a large system by using the methods considered in this work can be achieved with the help of speed-up algorithms such as those implemented in ORCA program [23]. In Table 2, we report an average single SCF cycle time, the MP2 calculation time, and the total calculation time of H2O...16T-Hz and H2O...3T-Hz systems when using SCS-MP2, double hybrid, hybrid and non-hybrid functionals methods. As expected, the computational cost of any methods involving MP2 calculation in a large system are much greater than those of conventional density functional methods. Moreover, one can see an important time saving upon invoking the speed-up algorithms such as RI-MP2 [21], RIJCOSX [25] and RI-J [26]. The RI-MP2 approximation reduces the MP2 computing time drastically. The 3T-Hz cluster with H2O adsorbate (332 basis functions) has the SCS-MP2 computational time reduced from 37 to 0.2 min. For a 16T-Hz cluster with H2O adsorbate containing 1691 basis functions, typical SCS-MP2 and B2PLYP calculations cannot be achieved on our quad core PC machine (Intel Q9450 chip @ 2.66 GHz with 4GB RAM). The MP2 calculation requires too many passes of integral transformation. Adopting the RI-MP2 approximation, the calculation becomes feasible with the MP2 part taking only a fraction of the total SCF calculation time. The RI-MP2 method also decreases the computing time of double-hybrid functional to be 1510 min which is in the same order of magnitude as that of conventional density func-tional. However, the conventional density functional can also be speed up by similar resolution of identity approximations. The RIJ-COSX and RI-J approximations for the hybrid functional and non-hybrid functional calculations, respectively, can speed up the selfconsistent field cycle by almost ten times. It would be interesting to invoke speed-up algorithm in both SCF and MP2 parts for the dou-ble-hybrid functional. The B2PLYP method with both RIJCOSX and RI-MP2 approximations indeed benefits from such computational saving with the total time for H2O...16T-Hz cluster calculation reduced to 561 min (see Table 2). This makes the double-hybrid functional competitive with conventional density functional method. These data suggest that one should adopt these speed up techniques to make a large system calculation feasible, notably for any methods involving MP2 calculation.

4. Conclusions

The adsorbate-zeolite binding energies calculated by using some density functionals with dispersion correction and spin-component scaled MP2 were compared against the benchmarking CCSD(T) results extrapolated to the complete-basis set limit sug-

gested by Zhao and Truhlar. The dispersion correction is important to obtain good estimation of binding energy. This is particularly crucial for the functional with Becke 88 exchange functional such as BLYP and B3LYP. The double-hybrid density functional model with dispersion correction is the most accurate model in this study with quality in rival to the best estimate binding energy of CCSD(T) with complete-basis set quality. Alternatively, the SCS-MP2 model can be used to calculate the counterpoise-uncorrected binding energy due to some fortuitous cancellation of errors. The resolution of identity approximation could be adopted to decrease the MP2 and SCF computational cost of both double-hybrid density functional and SCS-MP2 without losing any accuracy, hence making them practical methods for high accuracy adsorbate-zeolite calculations.

Acknowledgements

Financial supports from the Thailand Research Fund (RSA5180010) and the National Nanotechnology Center (NANOTEC) to NANOSIM laboratory are acknowledged. We thank Sila computing cluster, Ramkhamhaeng University and the high-performance computing cluster facility, NECTEC for computational facility.

[1] Y. Zhao, D.G. Truhlar, Acc. Chem. Res. 41 (2008) 157.

- Y. Zhao, D.G. Truhlar, J. Chem. Phys. 125 (2006) 194101.
 Y. Zhao, D.G. Truhlar, Theor. Chem. Acc. 120 (2007) 215.
 S. Grimme, J. Comput. Chem. 27 (2006) 1787.
 S. Grimme, J. Comput. Chem. 27 (2006) 1787.
 R. Ahlrichs, R. Penco, G. Scoles, Chem. Phys. 19 (1977) 119.
 J.-D. Chai, M. Head-Gordon, Phys. Chem. Chem. Phys. 10 (2008) 6615.
 P.C. Jha, Z. Rinkevicius, H. Agren, P. Seal, S. Chakrabarti, Phys. Chem. Chem. Phys. 10 (2008) 2715.
 L.-C. Lin, U. Rothlisberger, Phys. Chem. Chem. Phys. 10 (2008) 2730.
 C.A. Morgado, I.H. Hillier, N.A. Burton, J.J.W. McDouall, Phys. Chem. Chem. Phys. 10 (2008) 2706.
 S. Grimme, J. Chem. Phys. 124 (2006) 34108.
 F. Neese, T. Schwabe, S. Grimme, J. Chem. Phys. 126 (2007) 124115.
 T. Schwabe, S. Grimme, Phys. Chem. Chem. Phys. 8 (2006) 3398.
 T. Schwabe, S. Grimme, Phys. Chem. Chem. Phys. 9 (2007) 3397.
 P. Jurceka, J. Sponer, J. Cerny, P. Hobza, Phys. Chem. Chem. Phys. 8 (2007) 741.
 S. Velle, C. Tume, X. Rozanska, T. Kerber, J. Sauer, J. Am. Chem. Soc. 131 (2008) 816.

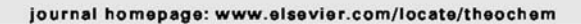
- 816. [18] Y. Zhao, D.G. Truhlar, J. Phys. Chem. C 112 (2008) 6860. [19] S. Grimme, J. Chem. Phys. 118 (2003) 9095. [20] J. Antony, S. Grimme, J. Phys. Chem. A 111 (2007) 4862. [21] F. Weigend, M. Haeser, H. Patzelt, R. Ahlrichs, Chem. Phys. Lett. 294 (1998) 143.

- F. Weigend, M. Haeser, H. Patzelt, R. Ahlrichs, Chem. Phys. Lett. 294 (1998) 143.
 F. Weigend, R. Ahlrichs, Phys. Chem. Chem. Phys. 7 (2005) 3297.
 F. Neese, ORCA an ab initio, Density Functional and Semiempirical program package, Version 2,635, University of Bonn, 2008.
 C. Tuma, J. Sauer, Phys. Chem. Chem. Phys. 8 (2006) 3955.
 R. Neese, F. Wennmohs, A. Hansen, U. Becker, Chem. Phys. Lett. 356 (2009) 98.
 R. Eickorn, O. Treutler, H. Oehm, M. Haeser, R. Ahlrichs, Chem. Phys. Lett. 240 (1995) 283.



Contents lists available at ScienceDirect

Journal of Molecular Structure: THEOCHEM





A DFT investigation of methanolysis and hydrolysis of triacetin

Taweetham Limpanuparb a, Kraiwan Punyain b, Yuthana Tantirungrotechai cd.

- Department of Chemistry, Faculty of Science, Mahidol University, Bangkok 10400, Thalland
 Department of Chemistry, Rucstry of Science, Naresuan University, Phitsanulok 65000, Thalland
 Kational Nontechnology Center (NANDTEC), National Science and Technology Development Agency, Pathumthani
 Theoretical Chemistry Laboratory, Faculty of Science, Mahidol University, Salaya, Nakhon Pathon 73170, Thalland and 12120 Thalland

ARTICLE INFO

Article history: Received 10 February 2010 Received in revised form 18 May 2010 Accepted 22 May 2010 Available online 26 May 2010

Keywords: Triacetin Hydrolysis Density Functional Theory

ABSTRACT

The thermodynamic and kinetic aspects of the methanolysis and hydrolysis reactions of glycerol triacetate or triacetin, a model triacylglycerol compound, were investigated by using Density Functional Theory (DFT) at the B3LYP/6-31++C(d,p) level of calculation. Twelve elementary steps of triacetin methanolysis were studied under acid-catalyzed and base-catalyzed conditions. The mechanism of acid-catalyzed methanolysis reaction which has not been reported yet for any esters was proposed. The effects of substitution, methanolysis/hydrolysis position, solvent and face of nucleophilic attack on the free energy of reaction and activation energy were examined. The prediction confirmed the facile position at the middle position of glycerol observed by NMR techniques. The calculated activation energy and the trends of those factors agree with existing experimental observations in biodiesel production.

© 2010 Elsevier B.V. All rights reserved.

1. Introduction

Triacylglyceride (TG) is a major constituent of naturally available oil and fat. The methanolysis, or transesterification, of triacylglyceride yields fatty acid methyl ester (FAME) and free glycerol as products. Alkaline methanolysis of triacylglycerol is a conventional process for biodiesel production from fresh vegetable oil owing to a very high conversion rate. This process makes use of a basic homogeneous catalyst such as KOH or NaOH [1]. The conversion rate is satisfactory provided that water and free fatty acid (FFA) contents in raw material are low [1]. This prerequisite prevents the hydrolysis reaction, the most important competing reaction, which yields soap as a product.

Methanolysis of triacylglycerol can be catalyzed by acid but with slower rate of conversion. Under acidic condition, the soap production is avoided and the esterification of FFAs which are found with high percentage in waste vegetable oil can take place simultaneously. However, this generally slow conversion rate of acid-catalyzed transesterification requires a rather high temperature condition [2].

We believe that the basic understanding on the metha and its competing hydrolysis reaction of triacylglycerol compounds at the molecular level is essential for the development of

E-mail address: yuthana@nanotec.or.th (Y. Tantirungrotechai).

0166-1280/\$ - see front matter © 2010 Elsevier B.V. All rights reserved. doi:10.1016/j.theochem.2010.05.022

biodiesel production. With the use of glycerol triacetate or triacetin as triacylglycerol model compound, we investigate the reaction mechanism of the methanolysis and its competing hydrolysis reaction under acid- or base-catalyzed conditions. The triacetin molecule was considered in this work because it is the smallest compound in triacylglycerol family that contains all features of triacylglycerols. It undergoes three successive reactions until it becomes glycerol and releases three fatty acids or fatty acid methyl esters depending on the involved reaction. In this work, four types of reaction are considered: base-catalyzed hydrolysis (BH), base-catalyzed catalyzed methanolysis (BM), acid-catalyzed hydrolysis (AH) and acid-catalyzed methanolysis (AM). There exists proposed reaction mechanism for BH, BM and AH reactions of some small compounds in the literature [3-10]. They are all bimolecular, base- or acid-catalyzed, acyl-oxygen cleavage reactions proceeded via the formation and dissolution of a tetrahedral intermediate. Schematically shown for the based-catalyzed hydrolysis in Fig. 1, there are five important stationary structures along the reaction coordinate: reactant complex (RC), first transition state (TS1), tetrahedral intermediate (TI), second transition state (TS2) and product complex

The reaction mechanism of the based-catalyzed hydrolysis of esters has long been studied by several groups [3-9]. Zhan et al. reported the hydrolysis of methyl acetate in gas phase and solution phase with the solvents being represented explicitly or by the solvation model [7,8]. In gas phase, five stationary structures along the reaction coordinate are identified with the dissolution of tetrahedral intermediate (TI) being the rate-determining step. This

Corresponding author at: Address: National Nanotechnology Center (NANO-TEC), National Science and Technology Development Agency, Pathumthani 12120,

Fig. 1. Schematic reaction mechanism of the based-catalyzed hydrolysis of methyl acetate (a) without and (b) with explicit water molecules proposed by Zhan et al. [7,8]. The hydrogen bond shown by dash line helps facilitate this reaction.

rate-determining step agrees with the experimental observation [11]. On the other hand, with the combination of four explicit solvent molecules and implicit solvent, only four stationary structures are reported. It was found that the RC structure in solvent phase is less stable than the separated reactants. It was then excluded from the calculation and the energy barrier was taken directly from the difference in energy of TS1 and separated reactants [6,8]. Zhan and Landry further reported the alkaline ester hydrolysis of cocaine and revealed that the face of nucleophilic attack can play a role on the reaction kinetics [6]. The energy barrier difference for the attack at the Si and Re faces of cocaine molecule is ~1 kcal/mol.

At least two reports exist on the mechanism of basemethanolysis of methyl acetate based on the previous hydrolysis work of Zhan and coworkers [12,13]. The dissolution of tetrahedral intermediate does not facilitate by the proton transfer as in the hydrolysis counterpart. Theoretical studies of alkaline methanolysis of vegetable oil in the literature are rather limited. Om Tapanes et al. conducted an experiment and theoretical studies of biodiesel formation from Jatropa curcas oil [14]. With the intention to clarify the existence of one or two tetrahedral intermediates along the reaction pathways of base-catalyzed methanolysis, the authors investigated the reaction pathways of monoglyceride by using the semi-empirical AM1 model. Only one tetrahedral intermediate was observed in their calculation. The dissolution of this tetrahedral intermediate was found to be the rate-determining step. The authors attribute the difference between the kinetics of the methanolysis and the ethanolysis to the alkoxide formation step. They also assume some similarity between each successive stage of conversion from triglyceride to glycerol. Asakuma et al. consider the difference between each stage of conversion in details [15]. Three different successive pathways for the base-catalyzed transesterification of various vegetable oil were proposed and investigated by using the HF/STO-3G method. Several alkoxides were considered in their work. The activation energy was found to be decreasing with the alkoxide size. Almost no variation of the activation energy with the carbon chain length of fatty acid was observed. The authors conclude that middle ester bond in the triglyceride is transesterified before the ester bond at the end position.

Recently Hori et al. reported the mechanism of gas-phase acidcatalyzed hydrolysis of methyl acetate in gas phase and solution phase modeled by explicit and implicit solvents [10]. The authors reported that the reaction proceeds only if when an explicit solvent molecule is included (see Fig. 2). In gas phase, the dissolution of TI is the rate-determining step. This was confirmed experimentally by several kinetic studies [16–20]. They noticed that explicit solvent molecules enhance the nucleophilicity of the attacking water which is a weaker nucleophile than hydroxide ion and facilitate the leaving of –OCH₃ group. Without additional water molecule, no stable TI structure was obtained [10]. According to this gas-phase mechanism, the barrier height of the second step is greater than that of the first step, implying that the leaving of –OCH₃ group with water-assisted proton transfer is the rate-determining step.

To the best of our knowledge, the reaction mechanism of the acid-catalyzed methanolysis has not yet been elucidated in the literature. Fox and coworkers reported an unsuccessful attempt to calculate acid-catalyzed methanolysis mechanism of methyl acetate [13]. They concluded that the methanol molecule could not get close to the carbonyl carbon enough to form a TI structure. This might be due to the neglect of explicit solvent molecule as in the case of acid-catalyzed hydrolysis reaction investigated by Hori group [10]. Therefore, we explored a plausible mechanism of acid-catalyzed methanolysis reaction in this work.

2. Computational details

Glycerol triacetate or triacetin, an ester of glycerol and three acetic acids, was chosen as a triacylglycerol model compound. As observed by Asakuma et al., the carbon chain length of fatty acid

Fig. 2. Schematic reaction mechanism of the acid-catalyzed hydrolysis of methyl acetate as proposed by Hori et al. [10].

plays minor role in the kinetics [15]. Therefore, the smallest acid side chain renders triacetin a practical model compound for computational study of biodiesel formation. It is utilized as a model compound in recent kinetic investigations of acid- and base-catalyzed methanolysis which aim to develop better catalysts for biodiesel synthesis [21,22]. These studies provide us with activation energies that can be used as a benchmark for our investigation.

Because triacetin can adopt several conformers, we conducted a preliminary search on the conformational energy landscape of triacetin. The two-dimensional conformational space based on two dihedral angles around the C-C bonds of the glycerol backbone was explored. Fig. 3 displays the mentioned dihedral angles and the numbering scheme used on the glycerol backbone. Nine minima and 18 first-order transition states of triacetin were identified on a two-dimensional conformational space. The most stable conformer is the one with two backbone OCCO torsional angles being trans and gauche. Our finding contradicted with reported MM2 result which predicted that both dihedral angles should be gauche plus and gauche minus for the global minimum [23]. We adopt the DFT global minimum structure of triacetin as an initial geometry for our study.

To elucidate the methanolysis/hydrolysis reactions of triacetin, we partitioned the whole reaction into three successive steps as

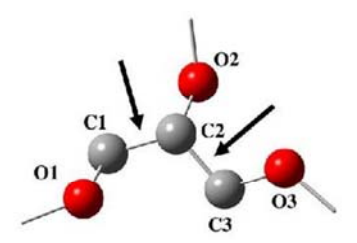


Fig. 3. The glycerol backbone of the most stable triacetin structure (H points outward at C2).

originally outlined by Yamasaki [24]. Fig. 4 illustrates 12 possible elementary steps to methanolyze or hydrolyze three ester linkages of triacylglyceride. Each step is essentially the removal of single acyl group by attacking nucleophile of which the reaction mechanism proceeds with tetrahedral intermediate as stated earlier. The form of nucleophile depends on the catalyst used. For acid-catalyzed reaction, the nucleophile is the neutral CH₃OH or H₂O molecule for methanolysis and hydrolysis reactions, respectively. During the reaction, the protonation occurs on the carbonyl oxygen of the ester substrate. For base-catalyzed reaction, we consider the CH₃O⁻ or OH⁻ ions as nucleophile for methanolysis and hydrolysis reactions, respectively. The nucleophile of this category also acts at the same time as basic catalyst. In both cases, the reaction proceeds through the nucleophilic substitution, then followed by either protonated ester or negatively charged nucleophile regeneration.

The geometries of all compounds in the scheme as well as that of RC, TS1, TI, TS2 and PC for all elementary steps were optimized by using the Density Functional Theory (DFT) at B3LYP/6-31++C(d,p) level. All stationary structures were verified by computing their hessian. The CPCM continuum solvation model was used to incorporate the solvent effect. In some case, explicit solvent molecules were included in the calculations. The reaction free energy and the activation energy for all 12 elementary steps were evaluated and compared with available experimental kinetics data of triacetin and vegetable oil [22,25–27]. All calculations in this work were performed by using the Gaussian 03 program [28].

3. Results and discussion

Table 1 summarizes average reaction free energies for the methanolysis and hydrolysis reactions of triacetin in the acidand base-catalyzed conditions. The reaction free energies were averaged from those of all 12 possible elementary steps (see Fig. 4 and Table 2). The hydrolysis of triacetin is slightly exergonic in gas phase (-0.46 kcal/mol) but becomes moderately exergonic

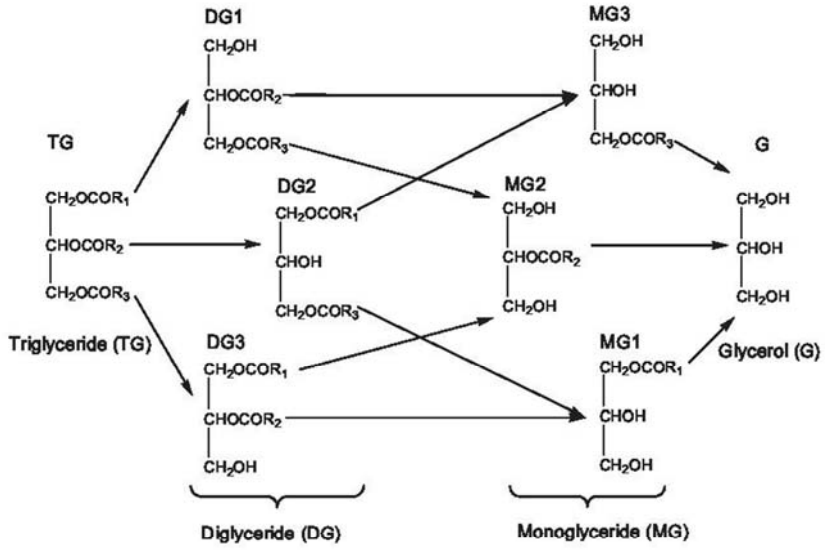


Fig. 4. All possible successive transformation steps for the methanolysis and hydrolysis of triacylglyceride to glycerol and three fatty acids or fatty acid methyl esters.

Table 1
Average reaction free energies for hydrolysis and methanolysis of triacetin (in keal/mol). The reaction free energies were averaged over 12 possible elementary steps.

<ΔG>/(kcal/mol)	Gas phase	cPCM ener	rgy at gas phase s	
		Water	Methanol	
Acid-catalyzed reactions (1) Protonation	-32.53	-5.72	-6.04	
Hydrolysis reaction	-0.46	-3.71	-3.52	
(2) Nucleophilic substitution	9.53	-5.86	-5.23	
(3) Protonated ester regeneration	-9.99	2.15	1,71	
Methanolysis reaction	2,15	2,80	2,69	
(2) Nucleophilic substitution	-0.63	-4.19	-3.70	
(3) Protonated ester regeneration	-1.53	1.38	1,02	
Base-catalyzed reactions				
Hydrolysis reaction	-0.46	-3.71	-3.52	
(1) Nucleophilic substitution	-45.19	-28.47	-28,59	
(2) Nucleophile regeneration	44.73	24.76	25.07	
Methanolysis	-2.15	-2.80	-2,69	
(1) Nucleophilic substitution	-21,02	-8.93	-9.23	
(2) Nucleophile regeneration	18.87	6.13	6.54	

Bold values signifies that these numbers are sum or average of the other.

in solution phase (~-4 kcal/mol). On the other hand, the reaction free energies for triacetin methanolysis are approximately the same for gas and solution phase (~-2 kcal/mol). From thermodynamics point of view, methanolysis is, therefore more favorable than hydrolysis in gas phase, but becomes less favorable than hydrolysis in solution phase. This discrepancy between gas and solution phase suggests that the solvents play an important role and should be included in the calculation to better reproduce experimental data. Although the reaction free energies in acidand base-catalyzed conditions are the same, the reaction free energies of the nucleophilic substitution in these two conditions are different. The corresponding energy in basic condition is greater

Table 2

Reaction free energies for 12 elementary steps of triacetin methanolysis (in kcal/mol) and their averages. The reaction free energies were averaged according to (i) the number of acyl substituents on glycerol backbone and (ii) the position on the glycerol backbone that methanolysis takes place.

	Gas phase	CPCM water	r	CPCM meth	anol
		Solvent phase structure	Gas phase structure	Solvent phase structure	Gas phase structure
MeQAc	0.00	0.00	0.00	0.00	0.00
TG→DG1	-1.56	-3.09	-3.02	-2,28	-2.81
TC→DC2	-3.41	-4.33	-4.72	-4.14	-3.75
TC→DC3	-2.45	-1,23	-2.44	-2.85	-1.91
DG1→MG2	-1.69	-1.82	-1.88	-1.40	-1.61
DG1→MG3	-2.96	-2.90	-3.69	-4.74	-2.86
DG2→MG1	-1.36	-0.19	-1.76	-0.87	-2.37
DG2→MG3	-1.14	-1.66	-1.99	-2.88	-1.92
DG3→MG1	-2.32	-3.29	-4.03	-2.16	-4,20
DG3→MG2	-0.80	-3.68	-2.46	-0.83	-2.51
MG1→G	-2.40	-2.46	-2.06	-2.13	-2.06
MG2→G	-3.91	-2.07	-3.63	-3.46	-3.75
MC3→C	-2.62	-0.99	-1,82	-0.12	-2.51
No. of acyl st					
TG→DG	-2.41	-2.81	-3.40	-3.09	-2.82
DÇ→MÇ	-1.65	-2.18	-2.65	-2.15	-2.58
MG→G	-2.9 1	-1.76	-2.52	-1 .90	-2,77
Position of m	ethanolys	ris			
1	-1.41	-2.65	-2.40	-2.03	-2.33
2	-3.06	-3.07	-4.03	-3.63	-3.64
3	-1.96	-0.98	-1 .99	-1.31	-2.10
Average	-2,15	-2.23	-2.80	-2.32	-2.69

Bold values signifies that these numbers are sum or average of the other.

in magnitude than those in acid condition. This is probably due to the anionic nature of involving species. The choice of either water or methanol solvents simulated by CPCM model hardly affects the reaction free energy.

fects the reaction free energy.

Table 2 also reports the effect of optimized geometries on the reaction free energy. By using the gas-phase and solution-phase optimized geometries, the reaction free energies including the CPCM solvation are generally very consistent. We therefore adopted the gas phase optimized geometries to reduce computational costs for the rest of this work.

The variation of the reaction free energies of 12 elementary methanolysis steps in Table 2 is believed to be due to three factors: (1) the number and position of acetyl substituents on glycerol backbone, (2) the nucleophilic attacking position on glycerol backbone that methanolysis or hydrolysis takes place, and (3) the solvent effect. These thermodynamic quantities computed in gas and solution phase in Table 2 can also be considered as the relative stability of triacetin derivatives with respect to glycerol and three methyl acetate molecules (see also Fig. S1 in Supplementary information). The reaction free energy of an elementary step depends on the stability of reactants and products which in turn depends on their structures, i.e. position that reaction takes place, and the number and position of acetyl substituents.

Judging from the reaction free energies, the gas phase reactions follow these trends: $MG \rightarrow G > TG \rightarrow DG > DG \rightarrow MG$ and position 2 > position 3 > position 1. In other word, the MG \rightarrow G is the most exergonic reaction compared to TG → DG and DG → MG processes and is the most thermodynamically favorable process. Regarding the substitution position on the glycerol backbone, the nucleophile prefers to attack at the position 2 or the middle position. On the other hand, in solution phase the reaction follows these trends: $TG \to DG > DG \to MG \sim MG \to G$ and position 2 > position 1 > position 3. The trend in the attacking position on glycerol backbone in the gas phase reflects the steric hindrance in triacylglyceride molecule, i.e. the position 2 or the middle position is the most steric. The greater the steric relief is, the more exergonic the reaction becomes. For the side positions, the position 3 is slightly more steric than the position 1 because the acyl substituent at positions 3 and 1 of glycerol backbone is gauche and trans to the middle group, respectively. This trend at the side position is reversed in the solution phase. In solution, we believe that the dipole moment determines this trend. In polar solvents, the acyl group at the position 1, which is trans to the middle position, results in partial cancellation of the dipole moment of the reactant, hence making it less sta-

ble than those with acyl group at the position 3.

The hydrolysis and methanolysis reactions under both acid- and base-catalyzed conditions can be divided into major steps depending on the reaction condition (see Table 1). Under acid condition, the ester is protonated first before undergoing a nucleophilic substitution. Finally, a product is deprotonated by transferring a proton to another ester reactant and, therefore, regenerating a reactive ester to undergo nucleophilic substitution in the next cycle. Under basic condition, the negatively charged nucleophile directly attacks the ester. Then the product abstracts a proton from reactants to regenerate negatively charged nucleophile again. As the proton transfer process is known to be very fast process, our focus is on the nucleophilic substitution which is believed to be ratedetermining step. Although the total reactions should have the same reaction free energy independent of the catalysts involved, the acid-catalyzed and base-catalyzed reactions differ greatly in the nucleophilic substitution step. Considering the reaction energy of this step, the hydrolysis and methanolysis reactions are more favorable in the base-catalyzed condition than in the acid-catalyzed condition. This observation is in line with the experimental observation that rate of methanolysis of vegetable oil in alkaline medium is about 4000 times faster than that in acidic medium

[2]. However, to compare with these experimental observations, the reaction energy barrier in acid- and base-catalyzed conditions must be obtained.

In the following subsections, detailed reaction mechanisms of the nucleophilic substitution step in acid- and base-catalyzed conditions, including the corresponding energy barriers, will be discussed.

3.1. Acid-catalyzed methanolysis (AM)

Two possible mechanisms for acidic methanolysis are considered. Based on a report that tetrahedral intermediate of the reaction could not be obtained [13], a one-step mechanism with a transition structure was calculated as illustrated in Fig. 5. The barrier height in both gas and solution phases is over 30 kcal/mol. This is unusually high and almost three times greater than the experimental value of ~11 kcal/mol for triacetin [22]. We thus proposed two-step mechanism comprising of RC, TS1, TI, TS2 and PC stationary structures. Initially, we tried to optimize the TI structure consisting of only the ester and attacking nucleophile. The attempt was unsuccessful because the nucleophile could not get close to the ester enough to form the TI structure. Our finding agrees with what reported previously in the literature [10,13]. Therefore, we adopted the approach of Hori et al. which adds an explicit solvent molecule to enhance nucleophilicity of nucleophile and to assist proton transfer [10]. Using this technique, we were able to calculate the reaction mechanism of acid-catalyzed methanolysis for methyl acetate as well as for all 12 elementary steps of triacetin (see Table 3). By setting the energy of RC structure as the reference, the average free energy of five stationary structures over 12 elementary steps is depicted in Fig. 6 along with the stationary structures of MG1 - G step as an illustrative example. The dissolution of TI structure is the rate-determining step of this mechanism.

Table 6 reports the activation energy of the triacetin methanolysis averaged over 12 possible elementary steps for different number of acetyl groups on glycerol backbone and different nucleophilic attacking position. The mechanism provides us with the activation energy of ~15 kcal/mol in gas phase and ~7 kcal/mol in solution phase. According to the table, the DFT underestimated the barrier energies in solution phase; this is due to the shortcoming of DFT on proton transfer process [29,30]. We therefore carried out Hartree–Fock energy calculation on DFT geome-

tries for comparison. The experimental TG \rightarrow DG activation energy of \sim 11 kcal/mol was found to lie in between average TG \rightarrow DG DFT and HF barrier heights of \sim 8 and \sim 14 kcal/mol.

In gas phase, the preferential nucleophilic attacking position predicted from the reaction free energy agrees well with those predicted from the energy barrier. The ester bond at the middle position is the most reactive and also releases the most energy. In this case, the more thermodynamically favorable a reaction is, the faster it proceeds. However, in solution phase, the acidic methanolysis at position 1 has the least activation energy. This suggests that a reaction in solvent is likely to occur at a position which is less sterically hindered, so that a nucleophile can easily approach the carbonyl carbon. To our knowledge, there has not been any experiment under acidic condition that considers the nucleophilic attacking position factor yet. Our prediction, therefore, remains to be tested by experiment.

Another factor that could affect the activation energy of acidcatalyzed methanolysis is the face of nucleophilic attack. This factor has already been reported to be rather small in the case of base-catalyzed hydrolysis [6]. We considered the acid-catalyzed methanol attack on the SI and Re faces of MG1. As reported in

Table 3

The free energy reaction profile of triacetin acid-catalyzed methanolysis in gas phase (in local/mol). The reaction proceeds through five stationary structures as outlined in Fig. 6. The face of nucleophilic attack is indicated in parenthesis.

	RC → TS1	→TI	→152	→PC	Activation energy (E _a)
MeOAc	11,24	-2,12	5.82	-16.64	14,94
TG → DG1 (Re)	11.63	-3.09	7.47	-43.07	16.01
TC → DG2 (Re)	7.92	-0.77	3.10	-36.59	10.25
TG → DG3 (Re)	12,49	-2.91	7.98	-43.95	17.56
DG1 → MG2 (Re)	12.93	-2.11	6.28	-44,31	17.11
DG1 → MG3 (Re)	6.66	-1.71	6.06	-44.00	11,00
DG2 → MG1 (Re)	12.19	-0.97	7.48	-43.58	18.70
DG2 → MG3 (Re)	11,29	-2.02	6.54	-37.11	15.81
DG3 → MG1 (Re)	6.92	0.20	5.70	-38.86	12.82
DG3 → MG2 (Re)	10.40	0.01	2.33	-34.13	12.73
MG1 → G (Re)	11.89	-3.21	6.16	-37.36	14.84
MG2 → G (Re)	8.38	-0.89	6.35	-39.08	13.84
MG3 → G (Re)	12.58	-2.17	7.11	-39.84	17.52
MG1 → G (SI)	11.55	-2,44	7.62	-41,21	16.73
MG2 → G (SI)	8.62	-4.90	9.40	-33.51	13.13
MG3 → G (SI)	14,30	-3.76	4.25	-36.36	14.79

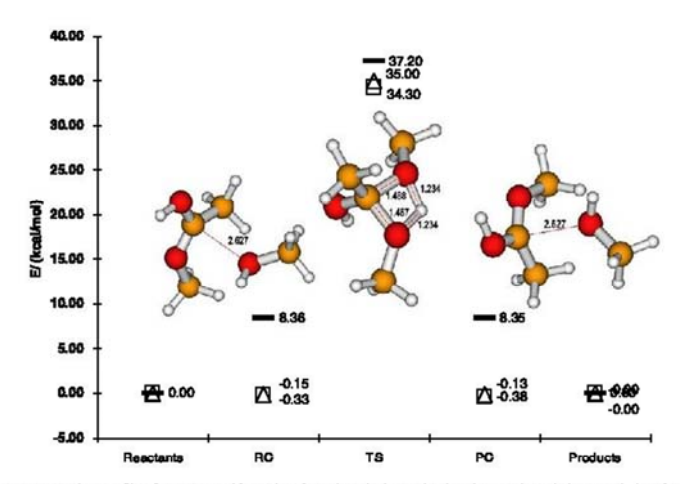


Fig. 5. Free energy reaction profile of one-step acid-catalyzed methanolysis mechanism in gas phase (-), water (\Box) and methanol (Δ).

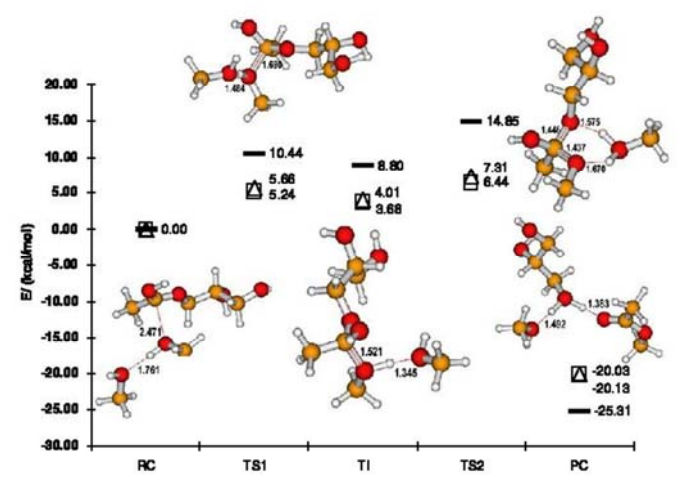


Fig. 6. Free energy reaction profile of acid-catalyzed methanolysis averaged over 12 elementary steps in gas phase (-), water (□) and methanol (△) environments. The geometries of MG1 undergoing acid-catalyzed methanolysis (Re face attack of methanol) are shown as a representative of the reaction.

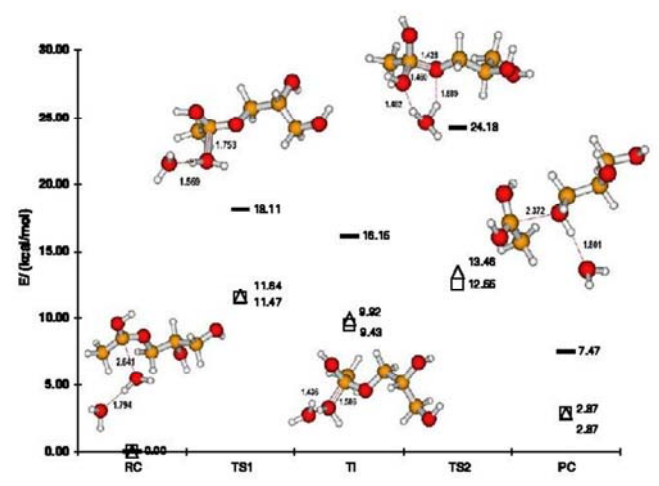


Fig. 7. Pree energy reaction profile of MGI acid-catalyzed hydrolysis (Re face attack of water) in gas phase (-), water (🗆) and methanol (△) environments.

Table 3, the difference in barrier height between the attack on Si and Re faces is about 3 kcal/mol in gas phase and 2 kcal/mol is solution phase.

3.2. Acid-catalyzed hydrolysis (AH)

By adopting initial geometry of stationary structures from AH mechanism reported for methyl acetate [10], the acidic hydrolysis mechanism of MG1 was summarized in Fig. 7. The rate-determining step is the dissolution of TI which is similar to the acid-catalyzed methanolysis mechanism. The MG1 activation energy for AH reaction of about 13 kcal/mol is comparable to the experimental activation energy of methyl acetate which is reported to be 16 kcal/mol [31].

As there are several factors that affect acid-catalyzed methanolysis and hydrolysis mechanism, the role of nucleophile, explicit and implicit solvent molecule on the activation energy were reported in Table 4. The activation energy of acid-catalyzed hydrolysis process is greater than that of methanolysis, implying that methanol is a better nucleophile than water. Methanol is also a better facilitating solvent compared to water as it results in a lower activation energy. The acid-catalyzed methanolysis of triacetin hence proceeds considerably faster than its corresponding hydrolysis reaction judging from these two observations. An implicit water model decreased the activation energy by about 1 kcal compared to those calculating with the methanol model. This reduction is however small compared to 3–7 kcal/mol difference originated from the choice of nucleophile and explicit solvent. Therefore the explicit solvent treatment,

Table 4 The activation energies for acid-catalyzed reaction of methyl acetate (MeOAc) and MG1 calculated with different nucleophile, facilitating solvent and implicit CPCM solvent. The energies were reported in terms of Gibbs free energy (in kcal/mol).

Ester	Gas phase	Implicit Sc	lvent	
Nucleophile/explicit solvent	50.WM 521112001	Water	MeOH	
MeOAc			11111111111	
MeOH/MeOH	14.94	6.54	7,41	
MeOH/H ₂ O	20.81	9.49	10.50	
H ₂ O/MeOH	18.19	10.83	11,20	
H ₂ O/H ₂ O	24.61	12.45	13.24	
MC1 → C (Re)				
MeOH/MeOH	14.84	6.51	7.61	
MeOH/H ₂ O	21,01	9.61	10.92	
H ₂ O/MeOH	17.31	9.83	10.37	
H ₂ O/H ₂ O	24.18	12.55	13.46	

Table 5 The free energy reaction profile of triacetin base-catalyzed methanolysis in gas phase (in kcal/mol). The reaction proceeds through five stationary structures as outlined in Fig. 8. The face of nucleophilic attack is indicated in parenthesis.

	RC → T\$1	→П	→152	→PC	Activation energy (E ₀)
MeOAc	2,11	-4.50	4.50	-2.09	2,11
TG → DG1 (Re)	2.00	-9.82	-1.62	-6.10	2.00
TG → DG2 (SI)	4.27	-14.71	-2.62	-4.01	4.27
TG → DG3 (SI)	1.93	-7.40	-1.58	-0.57	1.93
DG1 → MG2 (SI)	1.95	-15.11	10.74	-7.56	1.95
DG1 → MG3 (SI)	5.96	-11,17	-4.13	-3.19	5.96
DG2 → MG1 (Re)	3.39	-7.25	1.91	-7.71	3.39
DG2 → MG3 (Re)	5.28	-7.05	2.56	-2.49	5,28
DG3 → MG1 (SI)	6.47	-18.84	6.07	-15.15	6.47
DG3 → MG2 (Re)	1.84	-12.01	3.25	-4.24	1.84
MG1 → G (Re)	2.83	-2,52	0.68	-3.91	2.83
$MG2 \rightarrow G(SI)$	0.14	-10.14	3.02	-13.02	0.14
MG3 → G (Re)	1.91	-3.42	3.27	-4,20	1.91

even with the minimal amount of solvent molecules, is a prerequisite to a correct description of this reaction.

As the dissolution of TI structure coupled with the water-assisted proton transfer is the rate-determining step for both acid-catalyzed methanolysis (AM) and hydrolysis reactions (AH) of triacetin, the proton tunneling effect that was neglected so far might significantly reduce the calculated activation energy of this step. A rough estimation of the proton tunneling correction obtained from the Wigner expression at 298.15 K is less than 1 kcal/mol [6,32,33]. This number is in agreement with an earlier

study on base-catalyzed hydrolysis (BH); it also confirms that the second step of AM and AH is still the rate-determining step as the proton tunneling correction is too small to reverse the relative degree of barrier heights of these two steps [8].

3.3. Base-catalyzed methanolysis (BM)

The stationary structures and their corresponding energy along the reaction coordinate for 12 successive steps of the base-catalyzed methanolysis of triacetin were obtained with the help from mechanisms reported by Fox et al. and Chen and Brauman [12,13]. Table 5 summarizes the free energy reaction profile of triacetin base-catalyzed methanolysis in gas phase while Table 6 reports the activation energy in both gas and solution phases. In gas phase, the relative energy of five stationary points along the reac-tion coordinates is similar to those in the acid-catalyzed reaction. However the reactant complex (RC) structure becomes less stable than reactants in solution phase. We excluded the reactant complex from the energy barrier calculation of the first step and considered the energy difference between TS1 and separated reactants (SR) structures instead (see Fig. 8).

In contrast to the acid-catalyzed reaction, the formation of TI structure is the rate-determining step. According to the barrier height in Table 6, the calculations of this reaction were in qualitative agreement with the experimental observations (Refs. b and d in Table 6); the activation energy E_d follows this trend: DG \rightarrow MG \rightarrow TG \rightarrow DG \rightarrow MG \rightarrow G [26,27]. Although the experimental activation energy of 1-18 kcal/mol were obtained from triacylglyceride with long-chain fatty acids [25-27], our calculations on triacetin yield comparable values of 8-11 kcal/mol. These values fall into the range of activation energy observed in other triacylgly-cerides. We believe that triacetin is justified to be used as model compound representing the other triacylglycerides including those used as feedstock for biodiesel production.

3.4. Base-catalyzed hydrolysis (BH)

The optimized geometries and energies of MG1 species undergoing the base-catalyzed hydrolysis were calculated as illustrative case based on the proposed mechanism of methyl acetate by Zhan et al. [6-8]. The energy profiles in gas and solution phases were depicted in Fig. 8. The separated reactants energies were used to calculate the barrier height for the same reason as the base-catalyzed methanolysis reaction.

There are two additional solvated stationary structures, TI (water) and TS2 (water), for water-assisted dissolution of tetrahe-

Average activation free energies for the acid-catalyzed and base-catalyzed methanolysis (in kcal/mol) in gas phase and solvent phase. The experimental values are given for comparison

	Acid-catalyzed	reaction			Base-catalyze	d reaction		Experimental value	
	Gas phase	CPCM solv	rent		Gas phase	Gas phase CPCM solvent			
		Water	MeQH	HP*:MeOH		Water	MeOH		
No. of acyl sul	stituent							- 1111- I	
TG → DG	14.60	6.88	7.83	14.12	2.33	9.62	10.54	11.03b, 11.71c, 14.7d, 7.57c	
DG → MG	14,69	6.08	6.86	13.16	1.48	10.26	10.86	18.44°, 14.26, 9.94°	
MG → G	15.40	7.10	7.95	14.35	1.63	7.53	7.93	7.94°, 6.44, 1.42°	
Position of me	thanolysis								
1	14.85	5.73	6.65	13.91	2.99	6.89	7.40		
2	11.98	6.52	7.09	11.68	4.21	12.31	13.20		
3	17.72	7.36	8.39	15.49	2.30	9.05	9.55		
Overall	14.85	6.54	7.38	13.70	3.16	9.42	10.05		

^{*} HF, Hartree-Fock.

b Triacetin/methanol/H-SO4 [22].

<sup>Soybean oil/methanol/NaOH [26].
Palm oil/methanol/KOH [25].
Sunflower oil/methanol/KOH [27].</sup>

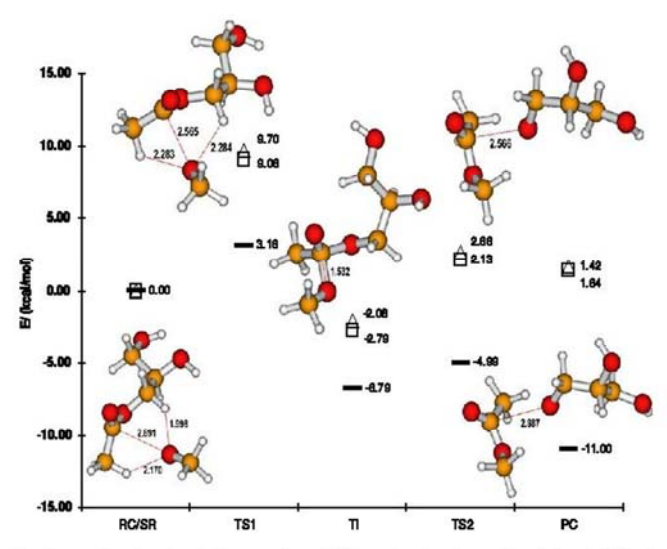


Fig. 8. Pree energy reaction profile of base-catalyzed methanolysis averaged over 12 elementary steps in gas phase (-), water (II) and methanol (\triangle) environments. The geometries of MG1 undergoing base-catalyzed methanolysis (Re face attack of methodide ion) are shown as a representative of the reaction.

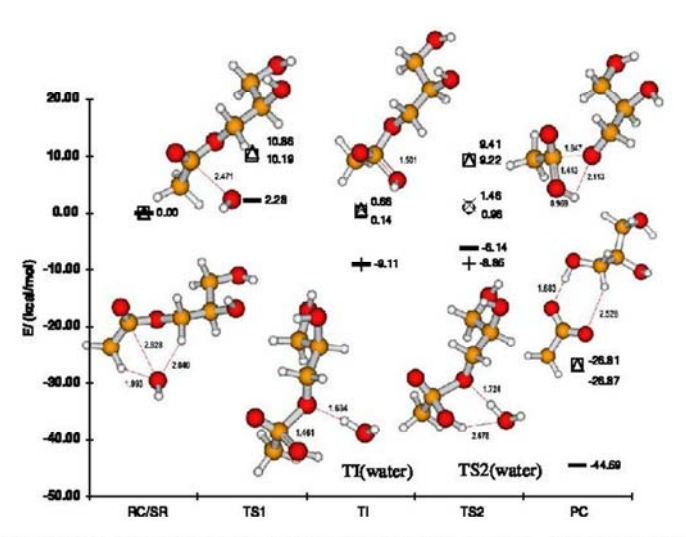


Fig. 9. Free energy reaction profile of MG1 base-catalyzed hydrolysis (Re face attack of hydroxide ion) in gas phase (-, +), water (\Box, \bigcirc) and methanol (\triangle, \times) environments. The energies of water-assisted proton transfer $(+, \bigcirc, \times)$ are shown along with explicit water associated Π (water) and Π (water) geometries.

dral intermediate. An explicit water molecule plays an important role in reducing the energy barrier in this step. This finding confirms what previously reports by Zhan et al. [6–8]. The reaction proceeds via this alternative pathway with the formation of TI structure being the rate-determining step. According to Fig. 8, the energy barrier of 10.19 kcal/mol in water agrees well with the experimental activation energy of 10.45 kcal/mol for the alkaline hydrolysis of methyl acetate in pure water by Fairclough and Hinshelwood [11]. The authors reported also that the activation energy of the same reaction in solution containing 71.3% ethanol

in water (w/w) is 15.0 kcal/mol. This indicates that the calculated solvent effect agrees qualitatively with the experimental observation that the barrier height increases as one increase the alcohol composition in solution.

4. Conclusions

We conducted series of DFT investigation for acid- and basecatalyzed hydrolysis and methanolysis reactions involving in biodiesel synthesis by using the triacetin as a model compound. Two acid-catalyzed methanolysis mechanisms were proposed and one-step mechanism with tetrahedral complex as the transition structure was ruled out based on the experimental observation. Then the mechanisms of 12 elementary steps of the acid- and base-catalyzed triacetin methanolysis were studied in detail. The calculated activation energies averaged over 12 elementary steps for different number of acetyl groups on triacetin and for the nucleophilic attacking position on the glycerol backbone are comparable to the available experimental values. The effects of the number of acetyl groups on triacetin and the solvent on the base-catalyzed methanolysis agree with the experiments. The preferential attacking position of methanol at the middle position of the glycerol backbone agrees well with the NMR experiment recently conducted by Jin et al. [34]. The thermodynamic trend in gas phase generally follows the kinetic trend while in solution phase only the kinetic trend is observed experimentally.

The gas phase activation energies of these four types of reac-tions (see Table 6 and Figs. 6-9) support general observation found in biodiesel production, i.e. the reaction proceed faster in basic condition, and the hydrolysis is a very important competing reaction under base-catalyzed condition but is unlikely to occur under acid-catalyzed condition. In solution phase, the activation energy of acid-catalyzed reaction decreases, while that of base-catalyzed reaction increases compared to the gas-phase condition. As the barrier height of acid-catalyzed methanolysis is likely to be underestimated by the present DFT functional, the activation energy of acid- and base-catalyzed reactions in solution phase could not be directly compared. The Hartree-Fock method was employed and found to overestimate the barrier height. The experimental activation energy was therefore found to lie in between the DFT and HF activation energies. The reaction mechanisms reported here cover all 12 elementary steps for converting triacetin successively to free glycerol and three methyl acetates (or three acetic acids) and could be further modified to include a body of heterogeneous catalysts into account.

Acknowledgements

T.L. gratefully acknowledges the Junior Science Talent Project (JSTP Grant No. 06-50-4R) and the Development and Promotion of Science and Technology Talent Project (DPST Grant No. 08/ 2547) for scholarship and research funding. Y.T. acknowledges financial support from the National Nanotechnology center (NANOSIM) and Thailand Research Fund (RSA5180010). We thank the HPC service, NECTEC for computational resources.

Appendix A. Supplementary data

Fig. S1 showing relative stability in terms of the free energy of transesterified species, TG+3MeOH, DG+2MeOH+MeOAc, MG+MeOH+2MeOAc, with respect to G+3MeOAc and B3LYP/6-31++G(d,p) molecular geometries for all compounds considered in this work are available in the online version at www. sciencedirect.com.

Supplementary data associated with this article can be found, in the online version, at doi:10.1016/j.theochem.2010.05.022.

- [1] G. Knothe, J. Van Gerpen, J. Krahl, The Blodiesel Handbook, AOCS Publishing,
- [2] B. Lotero, Y. Liu, D.B. Lopez, K. Suwannakarn, D.A. Bruce, J.G. Goodwin, Synthesis of biodiesel via acid catalysis, Ind. Eng. Chem. Res. 44 (2005) 5353-
- 5363.
 [3] P. Haeffner, C.-H. Hu, T. Brinck, T. Norin, The catalytic effect of water in basic hydrolysis of methyl acetate: a theoretical study, J. Mol. Struct. (THEOCHEM) 459 (1999) 85–93.

- [4] K. Hori, Theoretical study of reaction path via a hydrogen-bonded intermediate for the alkaline hydrolysis of esters in the gas phase, J. Chem. Soc. Perkin Trans. 2 (1992) 1629.
- [5] K. Hori, A. Kamimura, J. Kimoto, S. Gotoh, Y. Ihara, Theoretical study on the

- K. Hori, A. Kamimura, J. Kimoto, S. Gotoh, Y. Ihara, Theoretical study on the mechanism of ester hydrolysis in miceliar catalysis using model systems, J. Chem. Soc. Perkin Trans. 2 (1984) 2053.
 C.G. Zhan, D.W. Landry, Theoretical studies of competing reaction pathways and energy barriers for alkaline ester hydrolysis of cocaine, J. Am. Chem. Soc. 105 (2001) 1286–1301.
 C.G. Zhan, D.W. Landry, R.L. Omstein, Theoretical studies of fundamental pathways for alkaline hydrolysis of carboxylic acid esters in gas phase, J. Am. Chem. Soc. 122 (2000) 1522–1530.
 C.G. Zhan, D.W. Landry, R.L. Ornstein, Reaction pathways and energy barriers for alkaline hydrolysis of carboxylic acid esters in water studied by a hybrid supermolecule-polarizable continuum approach, J. Am. Chem. Soc. 122 (2000) 2621–2627.
 G.O. Andres, A.B. Pierini, R.H. DeRossi, Kinetic and theoretical studies on the
- [9] G.O. Andres, A.B. Pierini, R.H. DeRossi, Kinetic and theoretical studies on the chanism of intramolecular catalysis in phenyl ester hydrolysis, J. Org. Chem.
- Tri (2006) 7550-7656. K. Horl, Y. Ikenaga, K. Arata, T. Takahashi, K. Kasal, Y. Noguchi, M. Sumimoto, H. Yamamoto, Theoretical study on the reaction mechanism for the hydrolysis of esters and amides under acidic conditions, Tetrahedron 63 (2007) 1264—
- 1269.
 [11] R.A. Fairclough, C.N. Hinshelwood, The functional relation between the constants of the Arrhenius equation, J. Chem. Soc. (1937) 538–546.
 [12] X. Chen, J.J. Brauman, Proton exchange and transesterification reactions of accetate enolates with alcohols in the gas phase, J. Phys. Chem. A 109 (2005)
- acetate enolates with alcohols in the gas phase, J. Phys. Chem. A 100 (2003) 8553-8559.

 [13] J.M. Fox, O. Dmitrenko, La. Liao, R.D. Bach, Computational studies of nucleophilic substitution at carbonyl carbon: the SNZ mechanism versus the tetrahedral intermediate in organic synthesis, J. Org. Chem. 69 (2004) 7317-
- N.C. Om Tapanes, D.A. Gomes Aranda, J.W. de Mesquita Carneiro, O.A. Ceva Antunes, Transesterification of *Japanpha curcas* oil glycerides: theoretical and experimental studies of blodiesel reaction, Puel 87 (2008) 2286–2295.
 Y. Asakuma, K. Maeda, H. Kuramochi, K. Pulkul, Theoretical study of the transesterification of triglycerides to blodiesel fuel, Puel 88 (2009) 786–
- W.P. Huskey, C.T. Warren, J.L. Hogg, Substrate hydrophobicity and its influence on the transition-state structure for the water-catalyzed hydrolysis of acyl esters, J. Org. Chem. 46 (1981) 59-63.
 C.A. Lane, M.P. Cheung, G.P. Dorsey, The possibility of a cyclic mechanism for acid-catalyzed ester hydrolysis, J. Am. Chem. Soc. 90 (1968) 6492-6494.
 R.B. Martin, Mechanisms of acid hydrolysis of carboxylic acid esters and acid-catalyzed.

- mides, J. Am. Chem. Soc. 84 (1962) 4130-4136.

 R.B. Moodle, P.D. Wale, T.J. Whalte, The transition state in the acid-catalysed hydrolysis of benzamide, J. Chem. Soc. (1963) 4260-4288.

 K. Yates, Kinetics of ester hydrolysis in concentrated acid, Acc. Chem. Res. 4 (1971) 136-144.
- [21] D.E. Lopez, J.J.G. Coodwin, D.A. Bruce, E. Lotero, Transesterification of triacetin with methanol on solid acid and base catalysts, Appl. Catal. A 295 (2005) 97—
- D.B. Lopez, J.J.G. Goodwin, D.A. Bruce, Transesterification of triacetin with methanol on Nafion(R) add resins, J. Catal. 245 (2007) 381–391.
 D.G. Papageorgiou, I.N. Demetropoulos, I.E. Lagaris, P.T. Papadimitriou, How many conformers of the 1,2,3-propanetriol triacetate are present in gas phase and in aqueous solution?, Tetrahedron 52 (1996) 677–686.
 E. Yamasaid, The successive stages of the hydrolysis of triacetin, J. Am. Chem.
- Yamasald, The successive stages of the hydrolysis of triacetin, J. Am. Chem. c. 42 (1920) 1455–1468.

- E. Yamasaki, The successive stages of the hydrolysis of triacetin, J. Am. Chem. Soc. 42 (1920) 1455–1468.
 D. Damoko, M. Cheryan, Kinetics of palm oil transesterification in a batch reactor, J. Am. Oil Chem. Soc. 77 (2000) 1263–1267.
 H. Noureddini, D. Zhu, Kinetics of transesterification of soybean oil, J. Am. Oil Chem. Soc. 74 (1997) 1457–1463.
 G. Vicente, M. Martinez, J. Aracil, A. Esteban, Kinetics of sunflower oil methanolysis, Ind. Bing. Chem. Res. 44 (2005) 5447–5454.
 M.J. Prisch, G.W. Trucks, H.B. Schlegel, G.E. Scuseria, M.A. Robb, J.R. Cheeseman, J.A. Montgomery, T.V. Vreven, K.N. Kudin, J.C. Burant, J.M. Millam, S.S. Iyengar, J. Tomasi, V. Barone, B. Mennucci, M. Cossi, G. Scalmani, N. Rega, G.A. Petersson, H. Nakistuji, M. Hada, M. Ehara, K. Toyota, R. Puluda, J. Hasegawa, M. Ishida, T. Nakajima, Y. Honda, O. Kitao, H. Nakai, M. Klene, X. Li, J.E. Know, H.P. Hatchian, J.B. Cross, V. Bakken, C. Adamo, J. Jaramillo, R. Gomperts, R.E. Stratmann, O. Yazyev, AJ. Austin, R. Cammi, C. Pomelli, J.W. Ochtersid, P.Y. Ayala, K. Morokuma, G.A. Voth, P. Salvador, J.J. Dannenberg, V.G. Zaizrzewski, S. Dapprich, A.D. Danlels, M.C. Strain, O. Farks, D.K. Malick, A.D. Rabuck, K. Raghavachari, J.B. Foresman, J.V. Ortiz, Q. Cui, A.G. Baboul, S. Clifford, J. Cioslowski, B.B. Stefanov, G. Liu, A. Llashemo, P. Piskorz, L. Komaromi, R.L. Martin, D.J. Fox, T. Kelth, M.A. Al-Laham, C.Y. Peng, A. Nanayakikara, M. Challacombe, P.M.W. Gill, B. Johnson, W. Chen, M.W. Wong, C. Gonzalez, J.A. Pople, Gaussian O., Revision C.O., Gaussian, inc., Wallingford C.7, 2004.
 S. Sadbukhan, D. Munoz, C. Adamo, G.B. Scuseria, Predicting proton transfer
- C. Gonzalez, J.A. Popre, Gaussian.

 C. Gonzalez, J.A. Popre, Gaussian.

 C.E. Scuseria, Predicting proton transfer barriers with density functional methods, Chem. Phys. Lett. 306 (1999) 83—

 C. Gonzalez, J.A. Popre, Gaussian.

 C. Gonzalez, J. Gonzalez, J. Gonzalez, J. Popre, Gaussian.

 C. Gonzalez, J. Gonzalez, J.
- [30] P.R.M. Slegbahn, The performance of hybrid DFT for mechanisms involving transition metal complexes in enzymes, J. Biol. Inorg. Chem. 11 (2006) 695–

- W.B.S. Newling, C.N. Hinshelwood, The kinetics of the acid and the alkaline hydrolysis of esters, J. Chem. Soc. (1936) 1357–1361.
 R. Arnaud, N. Bugaud, V. Vetere, V. Barone, Role of polar and enthalpic effects in the addition of methyl radical to substituted alkenses: a Density Functional Study including solvent effects, J. Am. Chem. Soc. 120 (1998) 5733–5740.
- V. Barone, N. Rega, T. Bally, C.N. Sastry, Ring-opening reaction of cyclobutene radical cation: effect of solvent on competing pathways, J. Phys. Chem. A 103 (1999) 217-219.
 F.Jin. K. Kohel, H. Krishida, K. Tohji, T. Moriya, H. Enomoto, NMR spectroscopic study on methanolysis reaction of vegetable oil, Fuel 86 (2007) 1201-1207.

Helical Compounds Forming Gas-Phase Dimers: A Dispersion-corrected Density Functional Investigation

Pornthip Tongying, Thanasat Sooksimuang,† and Yuthana Tantirungrotechai*

National Nanotechnology Center, National Science and Technology Development Agency, Pathumthani, 12120 Thailand *E-mail: yuthana@nanotec.or.th

[†]National Metal and Materials Technology Center, National Science and Technology Development Agency, Pathumthani, 12120 Thailand

Received September 27, 2010, Accepted February 12, 2011

Chiral discrimination is the ability to distinguish one enantiomeric form over another. The differential binding interaction between two molecules with the same helicity and those with the opposite helicity was investigated by using dispersion-corrected density functional theory. [5]helicene, tetrahydro[5]helicene and the polar $D-\pi$ -A compounds, 3,12-dimethoxy-7,8-dicyano-[5]helicene and 3,12-dimethoxy-7,8-dicyano-tetrahydro[5]helicene were the monomers considered in this study. In gas phase, the dimeric interaction from two helical molecules with the opposite handedness is greater than from those with the same handedness. The stable configurations of such dimers were identified. The most stable configuration tends to be the one with maximum contact between monomers.

Key Words: Helicene, Dispersion-corrected density functional, Aggregate, Chiral discrimination

Introduction

Chirality is a very fundamental concept in molecular science. ¹⁻⁵ In chemistry, chirality usually arises from having chiral center, leading to a three-dimensional structure with a non-superimposible mirror image. The identification of the chiral configuration is very important because compounds with opposite chirality can have different biological activities. The receptor site built from stereospecific molecular unit binds with one chiral form of ligand rather than another due to their complementarity. ³⁻⁵ Such behavior is called chiral discrimination.

Helical structures exhibit chirality although they do not possess a chiral center. This is called helical chirality. Helical structures with right-handed or left-handed helicity are denoted P- and M-congurations, respectively. ²⁶ In this work, we investigated the differential binding interactions between gas-phase dimers formed from two monomers with the same helicity and from those with the opposite helicity. We selected [5]helicene and its derivatives as model compounds for our study.

Helicene is a chiral ortho-annulated π -conjugated system.⁷ Due to its helical structure and its conjugated nature, researchers are exploring its outstanding chirooptical properties for use as functional materials in many areas including nonlinear optics and organic light-emitting diode applications.⁸⁻¹¹ The helicene framework can be modified by incorporating other chemical elements or substituents.¹²⁻¹⁵ Sahasithiwat *et al.* modified the [5]helicene framework by incorporating electron donor and acceptor groups.¹⁶ The resulting D- π -A compound, 3,12-dimethoxy-7,8-dicyano-[5]helicene, is used as an emissive material for organic light emitting diodes. We include this compound in our study in

addition to [5]helicene (see Fig. 1(a)) due to its polar nature. We also consider tetrahydro[5]helicene and 3,12-dimethoxy-7,8-dicyano-tetrahydro[5]helicene which possess a carbon-carbon single bond on the 2^{nd} and 4^{th} rings of [5]helicene in this study (see Fig. 1(b)). These two compounds should have a smaller π - π interaction than the original helicene due to partial hydrogenation of the helicene framework.

Studying weakly interacting systems by quantum mechanical models can be a challenging task. In the case of conventional ab initio methods, at least the second-order Moller-Plesset perturbation theory (MP2) method which include electron correlation is required for a proper description of such systems. 17,18 This approach is too expensive to be practical for large systems like [5]helicene dimers. An alternative approach is to use the density functional theory (DFT) which is nowadays the method of choice for theoretical investigation of chemical systems. However, even the well-known B3LYP hybrid functional is not appropriate for treating weak interactions because of its incorrect long-range behavior in the exchange-correlation potential. 19 Many novel exchange-correlation functionals, such as the CAM-B3LYP20 and the Minnesota M06 and M08 functionals, 19,21-23 have been proposed to overcome this problem. Alternatively, a practical approach is to include an empirical dispersioncorrected term as originally proposed by Ahlrichs²⁴ and developed further for DFT by Grimme.^{25,26} The dispersioncorrected density functional theory (DFT-D) is a very convenient approach. This method is well suited not only for treating weak interaction but also for studying chemical reactions such as isomerization reactions.

Grimme et al. provide a clear perspective on the applications of dispersion-corrected density functional theory for supramolecular structures, aggregates and complexes of

Figure 1. The molecular structure of [5]helicene and tetrahydro [5]helicene monomers and their polar 3,12-dimethoxy-7,8-dicyano-derivatives. (a) [5]helicene, X, Y=H; 3,12-dimethoxy-7,8-dicyano-[5]helicene, X=OMe, Y=CN. (b) Tetrahydro-[5]helicene, X, Y=H; 3,12-dimethoxy-7,8-dicyano-tetrahydro-[5]helicene, X=OMe, Y=CN.

organic molecules.27 Mackie and DiLabio applied the DFT-D method to study interactions of several large polyaromatic hydrocarbon dimers. In their implementation, the authors optimized the carbon atom-centered effective core-type potential to correct the long-range behavior of the exchangecorrelation potential. Good agreement in the structure and binding energy with high-level benchmark data was observed.²⁸ Moellmann and Grimme investigated the dispersion effect for predicting the molecular crystal packing of a bis-thiophene derivative.²⁹ The dispersion-corrected DFT model predicts the crystal packing effect, the gas-phase structure, and the lattice energy of RESVAN, a bis-thiophene derivative, in good agreement with high-quality quantum chemical methods. However, they observed a near cancellation of intramolecular and intermolecular dispersion effects in the solid state structure. This results in the dispersion-uncorrected DFT model yielding a more reasonable solid state structure than the dispersion-corrected DFT model,

We selected the DFT-D model for calculating the differential binding interaction between M-M and P-M dimers constructed from [5]helicene and its derivatives (see Fig. 1). Our objectives are two-fold. First, several possible binding configurations of gas-phase dimers are identified. Second, the effect of structural modifications on the binding mode of these compounds is investigated. By comparing the most energetically stable form of the M-M and P-M dimers, some information on chiral discrimination of such compounds in gas-phase could be deduced.

There have been several reports on the chiral discrimination of helical structures including a recent review by Amemiya and Yamaguchi. 6,30,31 Yamaguchi et al. studied the chemistry of 1,12-dimethylbenzo[c]phenanthrene as a chiral building block.32 They concluded from several studies that one helix prefers another helix with the same helicity. Conclusions on chiral discrimination are usually drawn from solid state crystal structure, 30 from folding of helical oligomers or from complex formation with different molecules.3 Honzawa et al. studied the binding of 1,12-dimethylbenzo [c]phenanthrene, a basic [4]-helicene derivative, to righthanded calf thymus DNA by various spectroscopic and calorimetric techniques.33 By estimating the complex formation constant and the binding formation free energy, they observed a higher affinity between calf-thymus DNA with the righthanded (P)-helicene than with the left-handed (M)-helicene. Interestingly, the enthalpic contribution favors the (M)-

helicene more than the (P)-helicene by 2.1 kcal/mol. It appears that the entropic contribution results in the P form being more favorable in binding with calf thymus DNA than the M form. When accounting for chiral discrimination from crystal structure, there are some other factors such as cooperative hydrogen bonding³⁰ that play an important role in determining the crystal packing. Murguly *et al.* also observed different self-assembly behaviors in the crystal and in solution phases.³⁰ To avoid many-body effects, therefore, only the gas-phase aggregates were considered in our study. We consider the differential interaction energy between M-M and P-M gas-phase dimers as an indicator of chiral discrimination.

Methods

All calculations were performed using the ORCA program.³⁴ We consider the gas-phase helical dimers constructed from left-handed (M)-left-handed (M) and right-handed (P)-left-handed (M) pairs of monomers. The monomers are [5]helicene, tetrahydro[5]helicene, 3,12-dimethoxy-7,8-dicyano-[5]helicene and 3,12-dimethoxy-7,8-dicyano-tetrahydro-[5]helicene. Several initial configurations of M-M and P-M dimers were generated. These include, for example, head-head, head-tail, stack, antistack, slip and perpendicular configurations.

The geometries of dimer configurations were optimized by using the RI-BLYP-D/def2-SV(P) and RI-BP86-D/def2-SV(P) levels of calculation. Due to the large system size, the resolution of identity (RI) approximation was used to speed up the computation. We chose Grimme's implementation of DFT-D which includes an empirical 1/R6 term to capture the correct van der Waals dispersion interaction between monomers. 25,26 After the optimized configurations were identified, single-point energy calculations were performed using the same functional but with a much larger def2-TZVPP basis set35,36 and with the double-hybrid B2PLYP-D/TZVP method.37 The double-hybrid functional combines the conventional MP2 correction term with a hybrid functional. The Boys and Bernardi counterpoise correction scheme was used to remove the basis set superposition error (BSSE) in the interaction energy.38 The optimized dimeric configurations were identified and grouped together in terms of similar converged structures and interaction energies. The results are shown in Tables 1-4. Only the most favorable configurations for each dimer are shown in Figures 2(a)-(d) while all configurations are reported in the Supplementary Information.

Results and Discussion

Table 1 reports the M-M and P-M BSSE-corrected interaction energies of the non-polar [5]helicene dimers. Although several configurations were initially generated, the optimized structures fall into some dominant configurations. The M-M [5]helicene dimers fall into stack, antistack and slip configurations. We employed these terms to describe the relative configuration between the two monomers in a loose

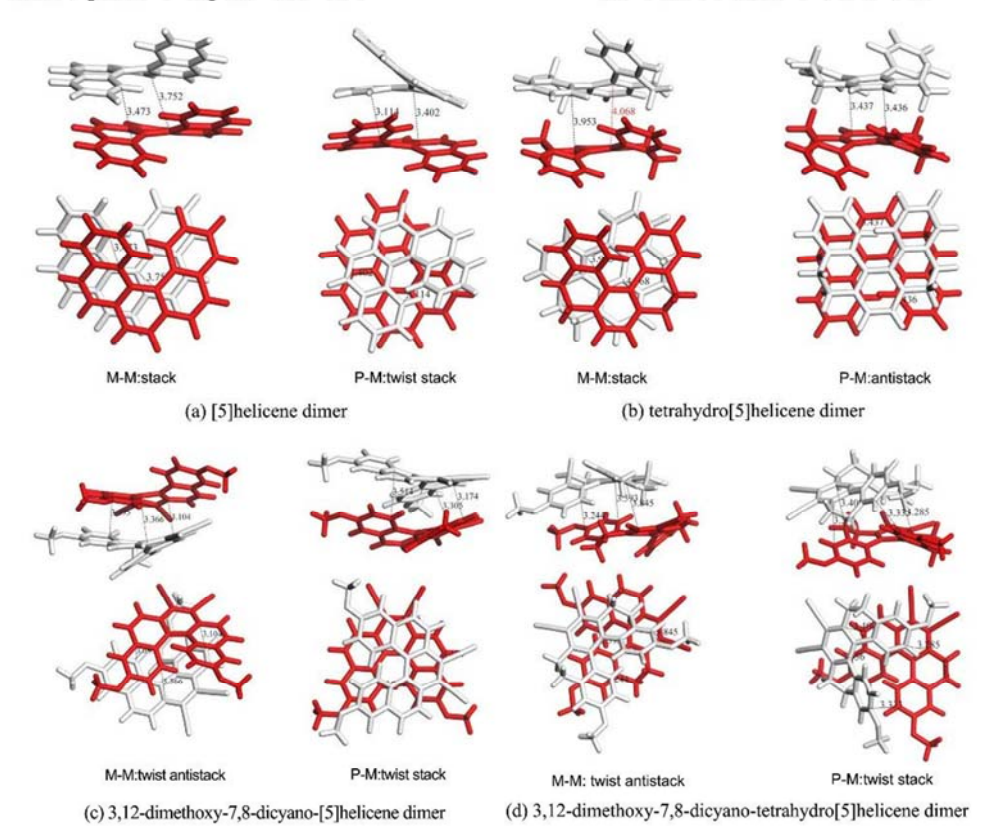


Figure 2. The most stable M-M and P-M gas phase configuration of (a) [5]helicene (b) tetrahydro[5]helicene (c) 3,12-dimethoxy-7,8-dicyano-[5]helicene (d) 3,12-dimethoxy-7,8-dicyano-tetrahydro[5]helicene dimets.

sense. The relative stabilities of the dimeric configurations from all calculation methods considered agree well with one another. The BLYP-D method cannot locate the less important slip configuration while the BP86-D can. However, this does not affect our conclusion because the most stable configuration is the stack configuration, i.e., one monomer above another with the end benzene rings pointing in almost the same direction (see Fig. 2(a)). It is also the configuration

Table 1. The M-M and P-M BSSE-corrected interaction energy (in keal/mol) of [5] believe dimers. See Figure 2a for graphical representation

	BP86-D/ def2-SV(P)	BP86-D/TZVPP// BP86-D/def2-SV(P)	BLYP-D/ def2-SV(P)	BLYP-D/TZVPP// BLYP-D/def2-SV(P)	B2PLYP-D/TZVP// BLYP-D/def2-SV(P)
			м-м		
stack	-15.3	-16.7	-13.3	-14,8	-13.8
antistack	-14.0	-15.1	-12.9	-13.7	-12.6
slip	-10.4	-11.6	n.a.	n.a.	n.a.
			P-M		
twist stack	-15.7	-16.9	-14.1	-15.1	-14.2
antistack	-14.4	-15.3	-12.8	-13.6	-13.2
stack	-13.8	-14.8	-12.2	-13.1	-12.6
slip antistack	-11.6	-12.6	-8.8	-9.7	-8.7
head-head	-11.4	-12.6	-7.7	-7.9	-7.1

found in the crystal packing.⁸ The antistack configuration which has the end benzene rings pointing in the opposite direction is the next most stable form. Although the energy difference between these two configurations is small, all methods including the definitive B2PLYP-D calculation confirm this trend. Due to the nature of the weak interaction, the interconversion between stack and antistack configurations should be possible. The configuration with one monomer on top of another has an increased contact area between the two monomers and hence there is a greater molecular interaction. To increase the molecular interaction further, the monomer slips slightly relative to the other in both stack and antistack configurations as a result of its nonplanar structure.

The most stable configuration of the P-M [5]helicene dimer is the twist stack configuration. A large degree of relative twist between the two monomers is observed in this configuration (see Fig. 2(a)). The monomer adopts this arrangement to increase the contact area and reduce the intermolecular distance. It turns out that the energetic interaction of the P-M [5]helicene dimer is slightly greater than that of the M-M dimer. The B2PLYP-D model predicts a differential binding energy of 0.4 kcal/mol This is in line with the observation made by Honzawa et al.33 In their complex formation study between a helicene derivative and calf thymus DNA, the enthalpic contribution to the binding constant was shown to favor opposite helicity while including the entropic contribution reversed the conclusion. Other identified stable configurations include antistack, stack, slip antistack and head-head configurations (see Supplementary Information). Considering the stack configuration which is found in crystal packing, the P-M dimer is less favorable than the M-M dimer by about 1.1-1.9 kcal/mol, Our result partly explains why helical compounds crystallize only in the enantiomeric pure form.30

Tetrahydro[5]helicene is a molecule with partial hydrogenation. This should reduce the π - π interaction found in [5]helicene and trigger hydrogen-hydrogen repulsion from saturated carbon atoms in the structure. In the case of the

tetrahydro[5]helicene dimer, the M-M dimer prefers the stack configuration while the P-M dimer prefers the antistack configuration (see Table 2 and Fig. 2(b)). Only a marginal difference in interaction energy between M-M and P-M forms is observed in such compounds. The BLYP-D method slightly favors the P-M form over the M-M form while with the BP86-D method this difference is more pronounced.

Comparing the [5]helicene and tetrahydro[5]helicene dimers, both M-M forms favor the stack configuration in which a helical monomer twists in the same direction as the other monomer thus forming another helical twist. On the other hand, the P-M dimer achieves maximum interaction by twisting around its intermolecular axis. For the tetrahydro[5]helicene dimer, the twist leads to the antistack configuration.

For 3,12-dimethoxy-7,8-dicyano-[5]helicene dimer, the M-M form prefers the antistack configuration with a further twist ('twist antistack', see Fig. 2(c)). The BSSE-corrected B2PLYP-D interaction energy is about -20.4 kcal/mol which is much greater than that of [5]helicene dimer (-13.8 kcal/ mol) (see Table 3). The methoxy and cyano substituents enhance the electrostatic interaction of the dimer. A simple electrostatic consideration also explains why the monomer twists itself further in such a dimer. This reduces the electrostatic repulsion from substituents of the same type and increases the attraction from substituents of the opposite type. The less stable configurations include stack, twist stack, slip antistack, perpendicular and slip configurations (see Supplementary Information). Table 3 also reports the BSSEcorrected interaction energies for each P-M dimeric configuration. The P-M dimer prefers the twist stack configuration (see Fig. 2(c)) and has an interaction energy of about -24 kcal/mol. In terms of differential interaction energy, the P-M gas-phase dimer is more stable than the M-M gas phase

A similar trend is also observed in 3,12-dimethoxy-7,8-dicyano-tetrahydro[5]helicene dimer (see Table 4, and Fig. 2(d)). For the B2PLYP-D method, the binding energy of P-

Table 2. The M-M and P-M BSSE-corrected interaction energy (in kcal/mol) of tetrahydro[5]helicene dimers. See Figure 2b for graphical representation

	BP86-D/ def2-SV(P)	BP86-D/TZVPP// BP86-D/def2-SV(P)	BLYP-D/ def2-SV(P)	BLYP-D/TZVPP// BLYP-D/def2-SV(P)	B2PLYP-D/TZVP// BLYP-D/def2-SV(P)
			м-м		
stack	-12,2	-13.9	-14.3	-15.7	-13.4
antistack	-12.3	-13.7	-12.2	-13.2	-11.8
slip	-9.3	-10.4	-7.2	-7.6	-6.8
head-head	-8.4	-9.4	-8.7	-9.2	-8.4
O-			P-M		
antistack	-15.0	-16.7	-14.4	-15,2	-13.4
stack	-14.3	-16.1	-13.9	-14.9	-12.6
twist stack	-12.3	-13.5	-12.3	-12.9	-10.8
slip stack	-8.9	-10.1	-10.4	-10.9	-9.2
head-head	-12,2	-13.3	-11.7	-12.0	-10.2

	BP86-D/ def2-SV(P)	BP86-D/TZVPP// BP86-D/def2-SV(P)	BLYP-D/ def2-SV(P)	BLYP-D/TZVPP// BLYP-D/def2-SV(P)	B2PLYP-D/TZVP// BLYP-D/def2-SV(P)
		1	м-м		
twist antistack	-22.3	-23.8	-20.5	-21.8	-20.4
stack	-18.8	-19.8	-17.1	-18.0	-17.5
twist stack	-18.5	-19.7	-17.3	-18.0	-17.0
slip antistack	-21.1	-22,2	-15.9	-17.0	-15.5
perpendicular	-9.0	-10.0	-10.8	-11.4	-10.6
slip	-11,2	-12,2	-10.6	-11.0	-10.6
		1	Р-М		
twist stack	-26.6	-28	-24.4	-25.8	-24.9
slip antistack	-20.7	-22,1	-19.1	-20.2	-19.6
slip stack	-15.1	-16.2	-14.1	-15	-15.2
stack	-13.5	-14.3	-14	-14.7	-14.2
perpendicular	-13.1	-14.7	-13.7	-14.6	-12.8
head-head	-12.3	-12.8	-12.0	-12,2	-11.2
slip	-9.8	-10.8	-10.1	-10.7	-9.8

Table 4. The M-M and P-M BSSE-corrected interaction energy (in kcal/mol) of 3,12-dimethoxy-7,8-dicyano-tetrahydro[5]helicene dimers. See Figure 2d for graphical representation

	BP86-D/ def2-SV(P)	BP86-D/TZVPP// BP86-D/def2-SV(P)	BLYP-D/ def2-SV(P)	BLYP-D/TZVPP// BLYP-D/dcf2-SV(P)	B2PLYP-D/TZVP// BLYP-D/def2-SV(P)
		1	м-м		
twist antistack	-21.4	-22.8	-19.8	-21.1	-17.7
twist stack	-15.6	-17.1	-15.5	-16.5	-14.1
perpendicular	n.a.	n.a.	-15.3	-16.5	-14.4
stack	-15.6	-17.4	-14.6	-15.7	-13.1
slip antistack	n.a.	n.a.	-13.1	-13.5	-10.5
slip	-13.1	-14.7	-13.3	-14.0	-11,4
head-head	-9.7	-12,2	-11.0	-12.3	-8.1
		(P-M		
twist stack	-19.3	-21.0	-20.7	-22,2	-18.8
slip antistack	-18.9	-20.8	-19.0	-20.1	-17.0
stack	-14.9	-16.6	-14.7	-15.8	-13.4
head-head	-15.9	-17.5	-13.6	-14.5	-12.6
slip stack	-12.3	-13.7	-12.2	-12.5	-10.0
side twist	-11,2	-12.7	-11.3	-12.0	-9.7
slip	n.a.	n.a.	-11.3	-12,1	-10.3
perpendicular	n.a.	n.a.	-7.9	-8.6	-6.7

M dimer is greater than that of the M-M dimer by -1.1 kcal/mol. The most stable configuration of M-M dimer is the twist stack while the P-M dimer prefers the twist antistack configuration. We observe a lower differential binding interaction between M-M and M-P forms of tetrahydro[5]helicene derivatives than in the case of the helicene derivatives. The enhancement of the interaction energy due to the donor and acceptor substituents is much less pronounced in this tetrahydro[5]helicene derivative than in the [5]helicene derivative. This might be due to the partial hydrogenation in the helicene framework that reduces the π electron delocali-

zation.

Some less stable configurations observed in this study, such as the head-head configuration, have also been observed experimentally. Murguly *et al.* synthesized and crystallized the hydrogen-bonded [7]helicene. As a result of the strong hydrogen bonding of the functional groups on the end benzene rings, the head-head dimer is formed as an entity in crystal packing.³⁰

The observation that, by considering the differential interaction energy between M-M and P-M forms, a helical molecule prefers to bind with another molecule of opposite handedness during gas-phase dimer formation might sound surprising at first. However, as mentioned earlier, several factors, such as the effects of crystal packing, substituents or entropic contributions, might play a role in favoring the binding of helical molecules with the same handedness. Our gas-phase calculation avoids any such influences and should give definitive energetic information on this type of dimer formation.

Finally, after the completion of this work, it came to our attention that favorable binding between two helical molecules with opposite handedness has been reported elsewhere. 39 Xu et al. conducted dialysis experiments to obtain the binding formation between thiahetero[7]helicene and lefthanded Z-DNA. The Z-DNA prefers binding with (P)helicene over (M)-helicene. Moreover, right-handed B-DNA converts into left-handed Z-DNA upon binding with (P)helicene. Further investigations on the helicene-DNA systems. of Honzawa et al. and Xu et al. are being carried out in our laboratory.

Conclusions

The gas-phase dimeric configuration of helicene derivatives were investigated by the DFT-D method to provide information on the differential binding interaction between helical molecules. In the absence of many-body effects, [5]helicene prefers P-M over M-M binding. The P-M dimer adopts the twist stack configuration while M-M favors the stack configuration. On modifying the helicene framework by partial hydrogenation, less differential binding is observed in the tetrahydro[5]helicene dimer. Adding electron withdrawing and donating groups into the helical structure increases the dimeric interaction. In such systems, there is a large twist between monomers. This is to lower electrostatic repulsion and increase electrostatic attraction. Our findings provide energetic information on the chiral discrimination process.

Acknowledgments. We thank the Thailand Research Fund (RSA5180010) and the National Nanotechnology Center (NANOSIM) for financial support. Computational facility at the high performance computing center (HPCC), large scale simulation research laboratory, the National Electronics and Computer Technology Center (NECTEC) is acknowledged. Finally, we thank Dr. Michael A. Allen of Physics Department, Mahidol University for his kind help on proofreading and manuscript editing.

Supplementary Materials Available. This information is available free of charge via the intermet at http://kcsnet.or.kr.

References

- 1. Lough, W.; Wainer, I. Chirality in Natural and Applied Science, 1st ed.: Blackwell: 2002.
- 2. Amouri, H.; Gruselle, M. Chirality in Transition Metal Chemistry:

- Molecules, Supramolecular Assemblies and Materials; Wilcy: 2009.
- 3. Meyers, R. A. Encyclopedia of Molecular Biology and Molecular Medicine; VCH Publishers: Weinheim, Germany, 1996.
- 4. Francotte, E.; Lindner, W. Chirality in Drug Research, Wiley-VCH: Weinheim, Germany, 2006.
- Mcycrs, R. A. Molecular Biology and Biote hensive Desk Reference; Wilcy-VCH: 1995.
- Amemiya, R.; Yamaguchi, M. Org. Biomol. Chem. 2008, 6, 26.
 Katz, T. J. Angew. Chem. Int. Ed. 2000, 39, 1921.
- 8. Morrison, D. J.; Trefz, T. K.; Piers, W. E.; McDonald, R.; Parvez,
- M. J. Org. Chem. 2005, 70, 5309.

 9. Botek, E.; Champagne, B. J. Chem. Phys. 2007, 127, 204101.

 10. Rajca, A.; Miyasaka, M. In Functional Organic Materials, Syntheses, Strategies and Applications; Wiley-VCH: Weinheim, Germany,
- Norel, L.; Rudolph, M.; Vanthuyne, N.; Williams, J. A. G.; Lescop,
 Norel, L.; Rudolph, M.; Vanthuyne, N.; Williams, J. A. G.; Lescop,
- C.; Roussel, C.; Autschbach, J.; Crassous, J.; Racau, R. Angew. Chem. Int. Ed. 2009, 49, 99.
- Alkorta, I.; Blanco, F.; Elguero, J.; Schröder, D. Tetrahedron: Asymmetry 2010, 21, 962.
- Abbate, S.; Bazzini, C.; Caronna, T.; Fontana, F.; Gambarotti, C.; Gangemi, F.; Longhi, G.; Mele, A.; Sora, I. N.; Panzeri, W. Tetrahedron 2006, 62, 139.
- 15. Urbano, A. Angew. Chem. Int. Ed. 2003, 42, 3986.
- Sahasithiwat, S.; Mophuang, T.; Menbangpung, L.; Kamtonwong, S.; Sooksimuang, T. Synth. Met. 2010, 160, 1148.
- 17. Cramer, C. J. Essentials of Compa and Models; John Wiley and Sons: UK, 2004.
- 18. Hobza, P.; Müller-Dethlefs, K. Non-Covalent Interactions: Theory
- and Experiment; Royal Society of Chemistry: UK, 2009.

 19. Zhao, Y.; Truhlar, D. G. J. Phys. Chem. A 2006, 110, 13126.

 20. Yanai, T.; Tew, D. P.; Handy, N. C. Chem. Phys. Lett. 2004, 393,
- 21. Zhao, Y.; Truhlar, D. G. Theor. Chem. Acc. 2007, 120, 215.
- 22. Zhao, Y.; Truhlar, D. G. Acc. Chem. Res. 2008, 41, 157. 23. Zhao, Y.; Truhlar, D. G. J. Chem. Theory Comput. 2008, 4, 1849.
- 24. Ahlrichs, R.; Penco, R.; Scoles, G. Chem. Phys. 1977, 19, 119.
- Grimme, S. J. Comput. Chem. 2004, 25, 1463.
 Grimme, S. J. Comput. Chem. 2006, 27, 1787.
- 27. Grimme, S.; Antony, J.; Schwabe, T.; Muck-Lichtenfeld, C. Org. Biomol. Chem. 2007, 5, 741.
- 28. Mackie, I. D.; DiLabio, G. A. J. Phys. Chem. A 2008, 112, 10968. 29. Moellmann, J.; Grimme, S. Phys. Chem. Chem. Phys. 2010, 12,
- 30. Murguly, E.; McDonald, R.; Branda, N. R. Org. Lett. 2000, 2, 3169
- 31. Carrillo, R.; López-Rodríguez, M.; Martín, V.; Martín, T. Angew. Chem. Int. Ed. 2009, 48, 7803.
- 32. Yamaguchi, M.; Okubo, H.; Hirama, M. Chem. Commun. 1996,
- Honzawa, S.; Okubo, H.; Anzai, S.; Yamaguchi, M.; Tsumoto, K.; Kumagai, I. Bioorg. Med. Chem. 2002, 10, 3213.
 Neese, F. ORCA an Ab Initio, Density Functional and
- Semiempirical Program Package, Version 2.6.35, University of Bonn, 2008.
- 35. Weigend, F.; Ahlrichs, R. Phys. Chem. Chem. Phys. 2005, 7, 3297.
- 36. Weigend, F.; Häser, M.; Patzelt, H.; Ahlrichs, R. Chem. Phys. Lett. 1998, 294, 143.
 37. Schwabe, T.; Grimme, S. Phys. Chem. Chem. Phys. 2007, 9, 3397.

- Boys, S. F.; Bernadi, F. Mol. Phys. 1970, 19, 553.
 Xu, Y.; Zhang, Y. X.; Sugiyama, H.; Umano, T.; Osuga, H.; Tanaka, K. J. Am. Chem. Soc. 2004, 126, 6566.

ภาคผนวกที่ 2 ผลงานที่กำลังอยู่ระหว่างการพิจารณาเพื่อตีพิมพ์และระหว่างการเตรียมต้นฉบับ

เฉพาะส่วน Title, Abstract and Acknowledgement

ผลงานที่กำลังอยู่ในระหว่างการส่งพิจารณาตีพิมพ์

6. Aphiradee Syananondh, Napaporn Youngvises, Panichakorn Jaiyong and

Yuthana Tantirungrotechai*

Binding Configurations of Cerium(IV) Complexes with Procaine and its Hydrolyzed Products: A Density Functional Investigation

Submitted to Computational and Theoretical Chemistry

7. Suthirat Yoopensuk, Pornthip Tongying, Kanidtha Hansongnern, Chaveng Pakawatchai, Saowanit Saithong, Yuthana Tantirungrotechai* and Nararak Leesakul*

Synthesis, Characterizations and Computational Studies of Photoactive Azoimine Dyes: 4-(2-pyridylazo)-N,N-diethylaniline and 4-(2-pyridylazo)-N,N-dimethylaniline

Submitted to Spectrochimica Acta Part A: Molecular and Biomolecular Spectroscopy

8. Pornthip Tongying, Suthirat Yoopensuk, Nararak Leesakul and Yuthana Tantirungrotechai*

Exploring Photochemistry of 2-(phenylazo)pyridine Dye By Using TDDFT/DFT Methods

Submitted to The Canadian Journal of Chemical Engineering

ผลงานที่กำลังอย่ในระหว่างเตรียมต้นฉบับ

9. Napaporn Youngvises*, Aphiradee Syananondh, Uboltip Satipchan, Thanatcha Chaida and Yuthana Tantirungrotechai

Surfactant enhanced sensitivity in flow injection analysis with cerium (IV) colorimetric reagent for determination of procaine hydrochloride

10. Nararak Leesakul*, Sirintip Pongampai, Proespichaya Kanatharana,

Prawit Sudkaew, Yuthana Tantirungrotechai, Chittanon Buranachai,

Screening Method for Flunitrazepam in Vodka and Tequila by Fluorescence Spectroscopy

Binding Configurations of Cerium(IV) Complexes with Procaine 1 and its Hydrolyzed Products: A Density Functional Investigation 2 3 5 6 Aphiradee Syananondha, Napaporn Youngvisesa, Panichakorn Jaiyonga and Yuthana Tantirungrotechaib* 8 9 Department of Chemistry, Faculty of Science and Technology, Thammasat University, Klong Luang, Pathumthani 12121 Thailand 0 ^bNational Nanotechnology Center, National Science and Technology Development Agency, 1 Klong Luang, Pathumthani 12120 Thailand 12 13 4 29 April 2011 Abstract We conducted density functional calculations on Ce(IV) complexes with procaine, a local anesthetic, and with its hydrolyzed products, para-amino benzoic acid (PABA) and diethylaminoethanol (DEAE) to find all binding configurations and locate the most stable binding configurations. This is to gain some understanding of the experiment of Youngvises et al. who conducted flow-injection based colorimetric analysis of procaine by cerium(IV) solution. By using the Ce(IV)F4(II2O)m (m=0,1,2) model fragment to bind with organic ligands, we found that the Ce(IV) binds favorably to the carbonyl oxygen with a bond angle of around 165°. Energetically, the Ce(IV)/PABA complex is the most stable configuration. The Ce(IV)/DEAE complex is less likely to occur in solution as the predicted electronic 10 excitation disagrees with experiment. The predicted electronic excitations of the Ce(IV)/procaine and Ce(IV)/PABA complexes fall into the same region and agree with 12 experiment. We believe that a Ce(IV) complex could initially form a complex with procaine 13 at the carbonyl oxygen and cause ester hydrolysis leading to a more stable Ce(IV)PABA complex in solution. 19 Acknowledgement 20 We thank Dr. Pornsawan Amornsakchai, Department of Chemistry, Naresuan University for providing computing facilities including access to Gaussian 09. Financial support from the 21 22 Thailand Research Fund (TRF Grant. RSA5180010) and the National Nanotechnology Center (NANOTEC) are acknowledged. N.Y. and P.C. acknowledge support from 23 24 Thammasat University and the Commission on Higher Education. Finally, we thank Michael

25

A. Allen for his proofreading.

Synthesis, Characterizations and Computational Studies of Photoactive Azoimine Dyes: 4-(2-pyridylazo)-N,N-diethylaniline and 4-(2-pyridylazo)-N,N-dimethylaniline

Suthirat Yoopensuk^a, Pornthip Tongying^b, Kanidtha Hansongnern^a,

Chaveng Pakawatchai^a, Saowanit Saithong^a,

Yuthana Tantirungrotechai^{b*} and Nararak Leesakul^{a*}

Department of Chemistry and Center for Innovation in Chemistry, Faculty of Science, Prince of Songkla University, Hat Yai, Songkhia, 90112, Thailand

*National Nanotechnology Center, National Science and Technology Development Agency, Thailand Science Park, Klong Luang, Pathumthant, 12120, Thailand

12 April 2011

Abstract

4-(2-pyridylazo)-N,N-dimethylaniline and 4-(2-pyridylazo)-N,N-diethylaniline, two photoactive azoimine dyes, were prepared from the reaction of 2-aminopyridine with N,N-dialkyl-1,4-nitrosoaniline at room temperature. Structural characterizations of these dyes using single crystal X-ray diffraction, H-NMR, elemental analysis, mass spectroscopy and IR spectroscopy have been carried out. The X-ray structure indicates a trans configuration around the azo group. The photochemical behaviour of these compounds differs from that of 2-phenylazopyridine, the non-dialkylamino substituent compound. The synthesized compounds show emission spectra at room temperature while 2-phenylazopyridine does not. The excitation spectra of these compounds differ from their absorption spectra which can be explained on the basis of the trans to cis photoisomerization which is supported by the TD-PBE0/6-31G(d,p) calculations. Both oxidation of the dialkylamino substituents (-NR2; R ■ -CH3 and -C2H3) and reduction of -N●N-/-N●N- and -N●N-/-N●N-2 were observed in the cyclic voltammogram indicating a π-acidity of both dyes.

Acknowledgements

N.L. acknowledges financial support from the Center for Innovation in Chemistry (PERCH–CIC), the Commission on Higher Education, and the Ministry of Education.

Ms.Sriwipha Onganusorn is acknowledged for supplying compound in ES-MS and CHN analysis. Y.T. is grateful to the National Nanotechnology Center (to NANOSIM) and the Thailand Research Fund (RSA-5180010) for financial support and HPC services, NECTEC for computing facilities. S.Y. is grateful for a TGIST scholarship

Exploring Photochemistry of 2-(phenylazo)pyridine Dye By Using TDDFT/DFT Methods

Pornthip Tongying¹, Sutherat Yoopensuk², Nararak Leesakul²

and Yuthana Tantirungrotechai^{1*}

¹Nanoscale simulation laboratory, National Nanotechnology Center, Thailand Science Park, Pathumthani Thailand

²Department of Chemistry, Faculty of Science, Prince of Songkla University, Songkhla Thailand

Abstract

- 2 The non-emissive behaviour of 2-(phenylazo)pyridine, azpy, observed in the fluorescence
- 3 experiment was explained by investigating its photoisomerization mechanism. By using the
- 4 Density Functional Theory and Time-dependent Density Functional Theory (DFT/TDDFT)
- 5 methods, the two-dimensional potential energy surfaces in the ground state, and the first and
- 6 second excited states which are relevant to the trans-to-cis isomerization were constructed.
- 7 The pathways related to the inversion, rotation and their concerted motion of the phenyl and
- 8 pyridyl groups around N=N bond were considered. The energy profiles depend not only on
- 9 the type of pathways but also on the moving group. The concerted inversion pathways show
- 10 the possibility of S_1/S_2 and S_0/S_1 conical intersections. The relaxation through such
- 11 intersections should increase the non-radiative transition rate to the extent that the compound
- 12 does not emit fluorescence.

1 Acknowledgements

1

- 2 We thank the National Nanotechnology Center (NANOTEC) and the Thailand Research
- 3 Fund (RSA-5100810) for financial supports. We thank the High Performance Computing
- 4 center at NECTEC and Dr. Pornsawan Amornsakchai of Naresuan University for providing
- 5 software access.

6

Surfactant enhanced sensitivity in flow injection analysis with cerium (IV) colorimetric reagent for determination of procaine hydrochloride

Napaporn Youngvises¹*, Aphiradee Syananondh¹, Uboltip Satipchan¹, Thanatcha Chaida¹, Yuthana Tantirungrotechai²

¹Department of Chemistry, Faculty of Science and Technology, Thammasat University, Pathum Thani, 12121 Thailand

²Nanoscale Simulation Laboratory, National Nanotechnology Center, National Science and Technology Development Agency, Pathum Thani, 12120 Thailand

Abstract

Flow injection analysis (FIA) with spectrometric detection was applied to determine procaine hydrochloride (PR) based on a reaction of procaine and cerium sulfate tetrahydrate (Ce (IV)) that produced the red compound. The sensitivity of this method can be increased by mixing sodium dodecyl sulfate (SDS) in the reaction mixture. Calibration graph was linear in the range of 1-150 mg L⁻¹ of PR with R² of 0.9998. The detection limit (3S/N) was 0.75 mg L⁻¹. Percentage recoveries and percentage relative standard deviation were 100-108 and 2.9, respectively. The proposed method was applied to determine PR in pharmaceutical preparation and compared to USP 2004. At 95% confidence, there was no significant difference between the results of both methods. The method should provide an accessible and ecofriendly way to determine PR in typical laboratory.

Acknowledgement

The authors would like to acknowledge Thammasat University, Commission on Higher education and Thailand Research Fund for financial support, and also thanks to chemistry department of Thammasat University and the National Nanotechnology Center (NANOTEC) for the facilities support in laboratory. Y.T. acknowledges the receipt of grant number RSA5180010 from Thailand Research Fund. Screening Method for Flunitrazepam in Vodka and Tequila by Fluorescence Spectroscopy

Nararak Leesakul^{4,*}, Sirintip Pongampai^b, Proespichaya Kanatharana⁴,

Prawit Sudkaew⁴, Yuthana Tantirungrotechai^c, Chittanon Buranachai^d,

- Department of Chemistry and Center for Innovation in Chemisty , Faculty of Science, Prince of Songkla University, Hat Yai, Songkhla, 90112, Thailand
- Department of Forensic Science, Faculty of Science, Prince of Songkla University, Hat-Yai, Songkhla, 90112, Thailand
- ⁴National Nanotechnology Center, National Science and Technology Development Agency, Thailand Science Park, Klong Luang, Pathumthani, 12120, Thailand
- Department of Physics, Faculty of Science, Prince of Songkla University, Hat Yai, Songkhla, 90112, Thailand

Abstract

Photochemistry offers a promising approach for detection of flunitrazepam in solutions. Owing to the basic structure of flunitrazepam, its protonated form restrictively exhibits distinctive optical properties from the deprotonated structure. Absorption and steady-state fluorescence of protonated and deprotonated flunitrazepams with a certain condition have been investigated. The red shift of wavelength of maximum absorption is obviously found in the protonated flunitrazepam. Its emissive fluorescence at 472 nm has been detected in colorless spirits (vodka and tequila) at room temperature. The 2 M perchloric acid is the most appropriated proton source. The protonated flunitrazepam was primarily characterized as acridone derivative by EIMS and TDDFT calculations.

Acknowledgements

N.L. would like to express our gratitude to Assoc.Prof.Dr.Chatchanok Karalai for his assistance in suggesting the scheme 1. Thanks to Dr.Chongdee Thammakhet, Dr.Thitima Rujiralai and Dr.Warakom Limbut for their comments during our group meeting. N.L. acknowledges for partially financial support from Center for Innovation in Chemistry (PERCH-CIC), Commission on Higher Education, Ministry of Education. S.P. is grateful for research assistance scholarship from Faculty of Science and research grant from Graduate school, PSU. Y.T. thanks National Nanotechnology Center (to NANOSIM), and Thailand Research Fund (RSA-5180010) for financial support and to Dr. Pornsawan Amornsakchai for access to Gaussian 09 software.